

CHIANTI – An atomic database for emission lines. XI. EUV emission lines of Fe VII, Fe VIII and Fe IX observed by Hinode/EIS.

P. R. Young^{1,2}

and

E. Landi²

ABSTRACT

A detailed study of emission lines from Fe VII, Fe VIII and Fe IX observed by the EUV Imaging Spectrometer on board the Hinode satellite is presented. Spectra in the ranges 170–212 Å and 246–292 Å show strongly enhanced lines from the upper solar transition region (temperatures $5.4 \leq \log T \leq 5.9$) allowing a number of new line identifications to be made. Comparisons of Fe VII lines with predictions from a new atomic model reveal new plasma diagnostics, however there are a number of disagreements between theory and observation for emission line ratios insensitive to density and temperature, suggesting improved atomic data are required. Line ratios for Fe VIII also show discrepancies with theory, with the strong $\lambda 185.21$ and $\lambda 186.60$ lines under-estimated by 60–80 % compared to lines between 192 and 198 Å. A newly-identified multiplet between 253.9 and 255.8 Å offers excellent temperature diagnostic opportunities relative to the lines between 185–198 Å, however the atomic model under-estimates the strength of these lines by factors 3–6. Two new line identifications are made for Fe IX at wavelengths 176.959 Å and 177.594 Å, while seven other lines between 186 and 200 Å are suggested to be due to Fe IX but for which transition identifications can not be made. The new atomic data for Fe VII and Fe IX are demonstrated to significantly modify models for the response function of the TRACE 195 Å imaging channel, affecting temperature determinations from this channel. The data will also affect the response functions for other solar EUV imaging instruments such as SOHO/EIT, STEREO/EUVI and the upcoming AIA instrument on the Solar Dynamics Observatory.

¹George Mason University, 4400 University Drive, Fairfax, VA 22030

²Naval Research Laboratory, Space Science Division, Washington, DC 20375

Subject headings: line: identification — atomic data — Sun: corona — Sun: UV radiation — Sun: transition region

1. Introduction

The iron ions are extremely important for the study of the solar corona as they give rise to many strong emission lines in the extreme ultraviolet wavelength range 90–400 Å that have been exploited for over 40 years (Gabriel et al. 1966; Phillips et al. 2008). Resonance lines of species such Fe IX, Fe XII and Fe XV have been selected for observation by EUV imaging instruments such as the EUV Imaging Telescope (EIT) on SOHO (Delaboudinière et al. 1995), the Transition Region and Coronal Explorer (TRACE, Handy et al. 1999), and the Extreme UltraViolet Imagers (EUVI, Howard et al. 2008) on the twin STEREO spacecraft. Spectroscopically, the iron lines have been measured by a range of space instrumentation, from the early Orbiting Solar Observatories (OSOs), through to the Skylab S082A spectrometer, the Coronal Diagnostic Spectrometer (CDS) on board SOHO (Harrison et al. 1995) and, most recently, the Hinode/EIS instrument (Culhane et al. 2007). The complexity of the iron ions’ atomic structure leads to many emission line pairs that are sensitive to electron density and, indeed, iron ions form most of the best coronal density diagnostics.

The iron ions Fe X to Fe XIV have received a lot of attention from observers and atomic physicists as they give rise to many strong lines in the solar spectrum. Fe VII–IX, by comparison, have few strong lines and atomic calculations are less common. Fe IX has a single very strong emission line at 171.07 Å and a density diagnostic involving two lines at 241.74 and 244.91 Å, but few other lines had been identified in the solar spectrum until Young (2009) presented four new line identifications based on Hinode/EIS spectra. Fe VIII gives rise to much weaker lines than the Fe IX–XIV ions and none of them have diagnostic potential, so the ion has received little attention. However, Fe VIII can make a significant contribution to the 195 Å imaging channel of the SOHO/EIT and TRACE instruments for polar plumes (Del Zanna et al. 2003) and coronal loops (Del Zanna & Mason 2003), while the high sensitivity of the Hinode/EIS spectrometer has led to Fe VIII lines being observed regularly (Young et al. 2007a). Fe VII is predicted to form around $\log T = 5.4$ (Bryans et al. 2009) where the emission measure of typical coronal features is much lower than for the higher temperature iron ions (e.g., Raymond & Doyle 1981). In addition, the atomic structure for Fe VII produces a large number of emission lines of relatively weak strength rather than a few strong lines such as found for the higher ionization stages of iron. These facts combine to make the observed Fe VII solar spectrum very weak compared to the other iron ions and

so it has been little studied.

The present work considers the lines of Fe VII, Fe VIII and Fe IX measured in the Hinode/EIS spectrum presented by Landi & Young (2009, hereafter Paper I), comparing measured intensities with predictions from atomic data in the CHIANTI atomic database (Dere et al. 1997, 2009) and investigating their diagnostic potential. The observed spectrum shows Fe VII–IX lines that are strongly enhanced over typical quiet Sun and active region conditions, and thus is ideal for studying lines that are normally too weak to be observed. In addition we discuss the formation temperatures of Fe VII and Fe VIII which appear to be discrepant with other ions.

2. Observations and data reduction

The Hinode/EIS data-set and data reduction method were described in detail in Paper I and are only summarized briefly here. The observation took place on 2007 February 21 at 01:15 UT, when the footpoint regions of active region AR 10942 were observed. Complete EIS spectra were obtained, and calibration was performed with the standard EIS routine EIS_PREP. Spectra from a strong brightening near the base of some coronal loops were averaged, taking care to adjust for spatial offsets between images obtained at different wavelengths. A complete line list from the final, averaged spectrum was presented in Paper I and a differential emission measure constructed. Emission line strengths from all ions formed in the range $5.4 \leq \log T \leq 6.0$ were analysed, except for the iron ions Fe VII–IX which are studied in the present work.

In the following sections we will refer to the differential emission measure (DEM) curve derived in Paper I, which was displayed in Fig. 8 of that work. In addition we also refer to the intensity images formed in various lines that are often valuable for determining the emitting species of unidentified lines or classifying blends. Fig. 1 of Paper I shows images from a wide range of ions belonging to different temperatures. The term “class” is used to group together emission lines for which the image morphology is similar to one of these reference images. For example class C lines are similar to Fe VII $\lambda 195.39$, class D lines similar to Fe VIII $\lambda 185.21$, etc. The complete list of temperature classes is given in Table 1 in Paper I.

3. Ion fraction comparison

The abundance of the emitting ion is a key ingredient in the analysis of the emission of spectral lines. Ion abundance calculations rely on ionization and recombination rates that

are continuously updated and improved both by laboratory measurements and by new *ab initio* calculations. Several data sets have been made available in the literature to provide reliable ion abundances as a function of temperature, a few of them published very recently.

Young et al. (2007b) noted that the temperature of maximum abundance, T_{\max} , of Fe VIII predicted by Mazzotta et al. (1998) appeared to be too low compared to observations. By comparing images obtained in several emission lines the authors demonstrated that the intensity distribution of Fe VIII, predicted to be found at $\log T_{\max} = 5.56$, was very similar to the intensity image of Si VII ($\log T_{\max} = 5.76$). Since, in terms of atomic structure, Si VII is a much simpler ion than Fe VIII, Young et al. (2007b) suggested the Mazzotta et al. (1998) ion fractions for Fe VIII were incorrect. Using the observations from the 2007 February 21 dataset we demonstrate that a similar effect is found for Fe VII. Figure 1 shows the intensity maps of the emitting region obtained with lines from Mg V-VII and Fe VII-VIII. The top row compares a Fe VII image with images from Mg V-VI, and the bottom row compares Fe VIII with Mg VI-VII. The intensity maps show that Fe VII and Mg VI images are very similar, implying similar T_{\max} values, while Fe VIII and Mg VII are also very similar. The Mazzotta et al. (1998) calculations, however, place Fe VII closer to Mg V and Fe VIII closer to Mg VI (see Table 1).

There have been several ion balance calculations performed over the past quarter of a century, and the Mazzotta et al. (1998) work is the most commonly used of recent years. Table 1 compares T_{\max} values for Mg VI-VII and Fe VII-VIII from these calculations, including three recent works (Bryans et al. 2006, 2009; Dere et al. 2009). The values for Mg VI-VII are remarkably consistent, however a marked decrease is found for both Fe VII and Fe VIII from the Arnaud & Raymond (1992) calculations onwards. Interestingly, the older T_{\max} values of Shull & Steenberg (1982) and Arnaud & Rothenflug (1985) for Fe VII and Fe VIII are more consistent with the intensity distributions shown in Figure 1.

In Fig. 2 we compare the ion fractions for Fe VII-IX as a function of temperature. Significant differences are found between the curves, but the largest ones take place with the iron ion update of Arnaud & Raymond (1992), that resulted in differences of up to one order of magnitude from the previous calculations. Investigating the reasons for this lies beyond the scope of the present paper, but there are two main avenues to be considered: 1) the rates used for Fe VII-IX are incorrect, or 2) some other process (e.g. dynamics, density effects) may be influencing the Fe VII-IX ion fractions.

Table 1. Values of the maximum abundance temperature $\log T_{\max}$ (in K) for Fe VII–VIII and Mg V–VII, from the seven most recent calculations available in the literature.

Data set	Mg v	Fe VII	Mg VI	Fe VIII	Mg VII
Shull & Steenberg (1982)	5.44	5.64	5.63	5.88	5.81
Arnaud & Rothenflug (1985)	5.43	5.61	5.63	5.82	5.80
Arnaud & Raymond (1992)	5.43	5.42	5.63	5.57	5.80
Mazzotta et al. (1998)	5.43	5.42	5.64	5.56	5.80
Bryans et al. (2006)	5.44	5.42	5.62	5.56	5.78
Dere et al. (2009)	5.45	5.41	5.63	5.61	5.78
Bryans et al. (2009)	5.45	5.42	5.63	5.62	5.78

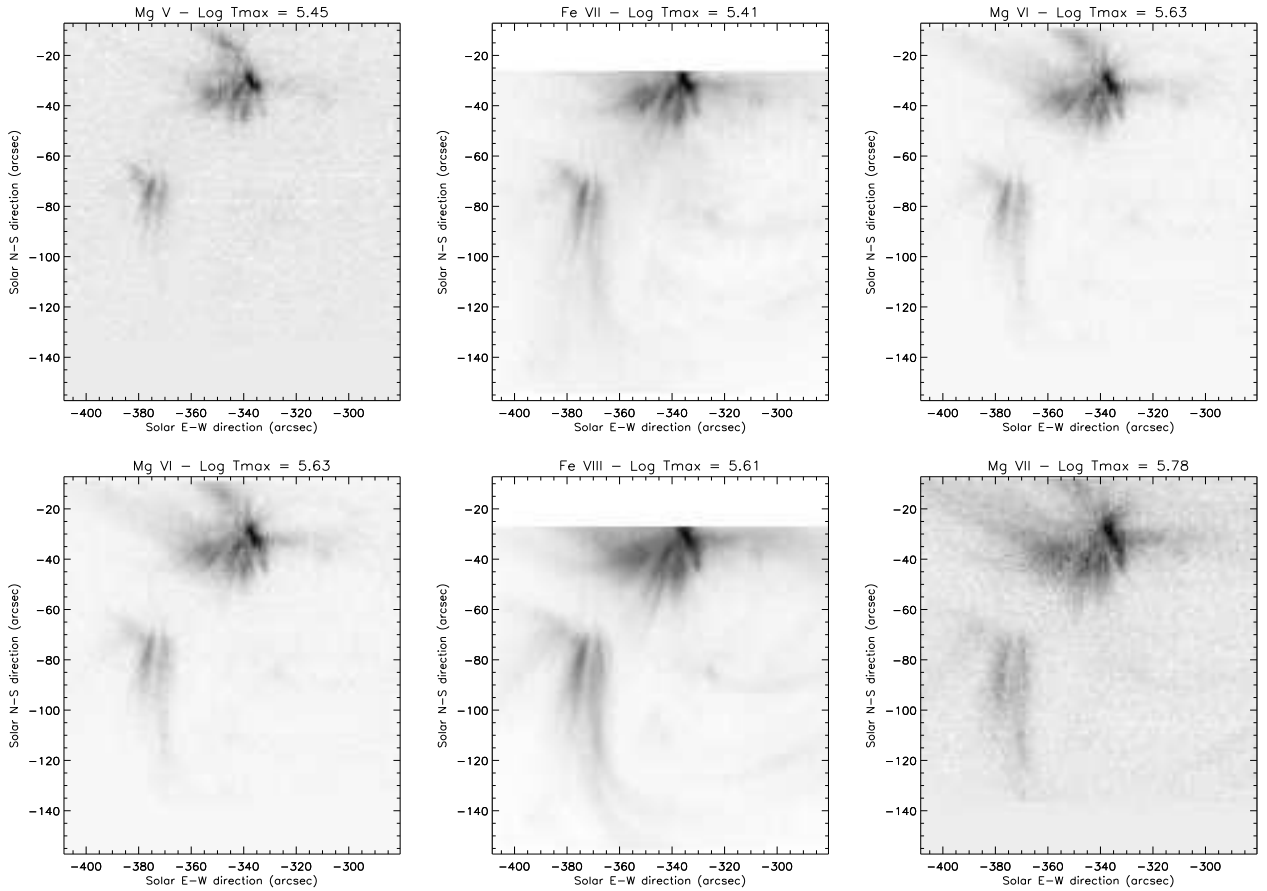


Fig. 1.— Intensity maps of a few selected ions. $\log T_{\max}$ is the temperature of maximum abundance of each ion, according to Mazzotta et al. (1998).

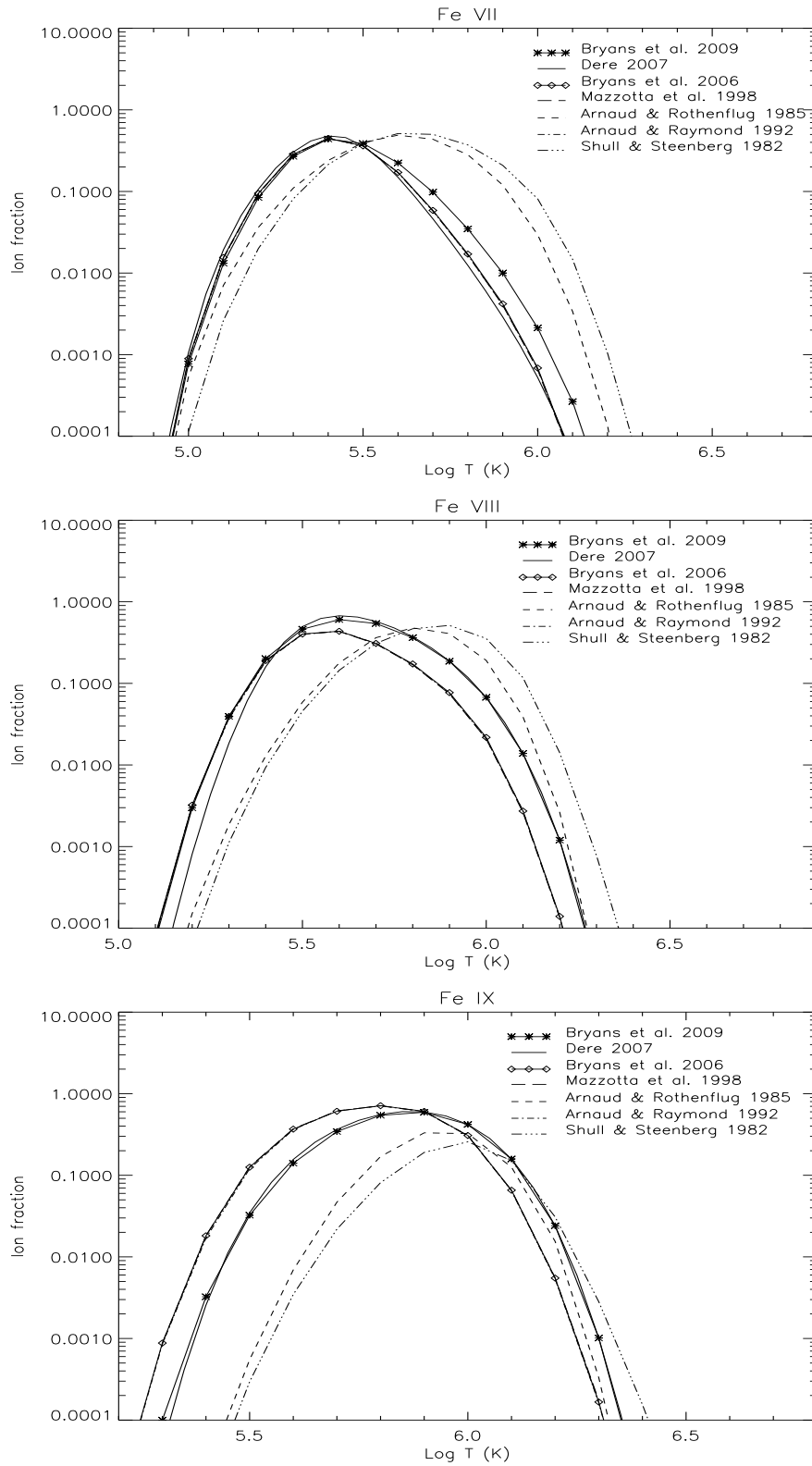


Fig. 2.— Comparison of ion fraction datasets for Fe VII, Fe VIII and Fe IX, using the most recent calculations.

4. Fe VII

Fe VII lines in the wavelength range 170–300 Å have received little attention from solar spectroscopists as the lines are generally very weak and there have been no atomic data available to model the line intensities. However, two extensive atomic calculations have been published in recent years that allow the lines to be modeled, while the launch of EIS in 2006 has allowed the routine measurement of parts of the 170–300 Å window at high resolution and high sensitivity. The spectrum presented in Paper I shows strongly enhanced lines of Fe VII compared to normal quiet Sun or active region spectra and so presents an excellent opportunity for comparing theory with observations.

Atomic data suitable for modeling electron-excited emission lines have been published by Zeng et al. (2005) and Witthoeft & Badnell (2008) and these are the first calculations that yield data for the excited configurations of the ion that give rise to the emission lines in the extreme ultraviolet. The Zeng et al. (2005) calculations were performed using the Flexible Atomic Code (FAC; Gu 2003) which uses the distorted wave approximation, while Witthoeft & Badnell (2008) performed a R-matrix calculation using the intermediate-coupling frame transformation (ICFT) method of Griffin et al. (1998). Generally R-matrix calculations are considered superior to distorted wave as they allow the resonant enhancement of collision strengths to be accurately modeled, although for excited configurations and high energies the results should be similar. Witthoeft & Badnell (2008) made a comparison with Zeng et al. (2005) and found good agreement for both radiative decay rates and collision strengths. For this work we choose to use the Witthoeft & Badnell (2008) for our atomic model.

The Witthoeft & Badnell (2008) data have been put into the format used by the CHIANTI database, and will be made publicly available in a future version of the database. For inclusion in CHIANTI the collision strengths have been fit with splines using the method outlined in Dere et al. (1997), while experimental energy levels have been taken from Ekberg (1981), Ekberg & Feldman (2003) and version 3 of the NIST database (Ralchenko et al. 2008). Many levels do not have experimental energies and for these the theoretical values of Witthoeft & Badnell (2008) were used. Some new and revised energy values are suggested from the present work and will be discussed below.

Since the atomic model constructed here is the first to yield intensity predictions for lines from excited configurations of Fe VII at typical coronal densities and temperatures, we outline briefly some of the properties of the lines in terms of diagnostic potential. Firstly, above densities of 10^9 cm^{-3} the nine ground configuration levels of Fe VII are in a quasi-Boltzmann distribution, and thus relative populations change little relative to each other above this value. This means that emission line ratios show little density sensitivity at typical coronal

densities of 10^9 – 10^{13} cm^{-3} . There is density sensitivity amongst some emission lines below 10^9 cm^{-3} which may be useful when studying coronal hole regions and specific diagnostics are highlighted in the sections below. The lines formed in the 170–300 Å range have a wide range of excitation potentials and so they can show significant temperature sensitivity. In the sections below we will highlight some useful temperature diagnostics and compare results from these ratios.

Ratios that are insensitive to the physical conditions of the atmosphere are also valuable as a check on the atomic physics parameters. In order to compare observed ratios with theory in these cases, we compute the theoretical ratio over the temperature range $\log T = 5.4$ – 5.7 at 0.05 dex intervals, and the density range $\log N_e = 8.0$ – 10.0 at 0.2 dex intervals. The listed theoretical ratio is then given as the average ratio over these ranges, and the “error” is the $2\text{-}\sigma$ value of the ratio over the ranges (Table 5). The temperature range has been chosen as $\log T = 5.4$ – 5.7 based on the discussion in Sect. 3. The density range chosen is based on the density measured from the Mg VII $\lambda 280.75/\lambda 278.39$ diagnostic (see Paper I) and allowing for up to an order of magnitude variation from this value.

Table 4 in Paper I listed line intensities predicted from the differential emission measure (DEM) curve and for most of the Fe VII lines the predictions are lower than the observed intensities by factors of 2–5. The Fe VII lines were not included when deriving the DEM curve since no previous check of the Fe VII atomic data has been performed. We believe the large underestimates of the intensities principally arise from the inaccurate ion fraction curve for Fe VII discussed in the previous section. The DEM predicted intensities include a convolution of the theoretical ion fraction curve and the DEM, and Figure 8 of Paper I shows that the DEM has a rather low value at $\log T = 5.4$, the Fe VII T_{max} value of Dere et al. (2009). If the ion fraction curve was shifted to around $\log T = 5.6$ – 5.7 , then it would sample larger values of the DEM and so increased predicted intensities would result. In the Fe VII discussions that follow we will generally not refer to the DEM intensity predictions for this reason.

Before embarking on our analysis of the observed EIS lines we first consider the measured EIS wavelengths of those transitions that have been identified previously. The line list of Ekberg (1981) is the only comprehensive one in the literature for the 170–300 Å range and was derived from laboratory spectra. Table 2 gives the Ekberg (1981) wavelengths and the measured EIS velocities from the present spectrum for those Fe VII lines from Ekberg’s list that are clearly identified in the EIS spectra and that are either unblended or provide the dominant contribution to blended lines. Table 6 in Paper I presented velocities from the cool ions presented in that paper and it was noted all ions between O IV ($\log T = 5.21$) and Mg VII ($\log T = 5.76$) have velocities of around 40 km s^{-1} . Taking the average velocity of

those lines identified to be unblended and without anomalies in Table 6 of Paper I, we derive a value of 40.4 km s^{-1} (using the velocities in the v_{ref} column of this table), with a standard deviation of 4.5 km s^{-1} . Fe VII belongs to this group of cool ions, even with the uncertainty in the ion fraction discussed in Sect. 3, and so we expect the ion’s line velocities to be consistent with the other cool ions. Therefore in Table 2 we indicate those emission lines for which the measured velocity is not consistent with the cool ion velocity of 40.4 km s^{-1} . We find 18 of the 25 lines show good agreement, giving confidence in the Ekberg (1981) measurements. The anomalous lines will be discussed in the following sections.

Since a number of new line identifications have been performed for Fe VII in this work, it is necessary to convert the measured wavelengths to rest wavelengths in order to derive new experimental energies for the upper emitting levels. For this we subtract the average cool ion velocity of 40.4 km s^{-1} from the measured wavelengths.

Table 2. Measured velocities for Fe VII lines.

Reference wavelength ^a (Å)	Velocity ^{b,c} (km s ⁻¹)
176.744	30.5 ± 10.9
182.071	46.1 ± 16.8
182.740	24.6 ± 14.7◁
183.539	44.1 ± 11.1
183.825	39.1 ± 8.6
184.752 ^d	40.6 ± 9.1
184.886	58.4 ± 9.8◁
185.547	43.6 ± 8.5
186.657	56.2 ± 12.9◁
187.235 ^e	44.8 ± 8.3
187.692	35.1 ± 8.6
188.396 ^f	44.5 ± 9.5
188.576	42.9 ± 9.0
189.450	49.1 ± 8.1◁
195.391	36.8 ± 7.7
196.046	42.8 ± 7.9
196.423	53.4 ± 7.9◁
201.855	47.5 ± 7.9
207.712	44.7 ± 8.1
208.167	46.1 ± 17.3
265.697	46.3 ± 6.6
289.678 ^g	50.7 ± 6.8◁
289.831 ^g	54.8 ± 6.1◀
290.307 ^g	39.2 ± 5.9
290.756 ^g	36.1 ± 5.6

^aFrom Ekberg (1981).

^bErrors represent the EIS measurement errors combined with the $\pm 0.005 \text{ \AA}$ errors on the Ekberg (1981) reference wavelengths.

^cA \triangleleft symbol beside the velocity measurement indicates that it is discrepant with the average cool line velocity of $+40.4 \text{ km s}^{-1}$ by $> 1\sigma$; a \blacktriangleleft indicates a discrepancy of $> 2\sigma$.

^dBlended with Ne v $\lambda 184.735$ and Fe XI $\lambda 184.803$.

^eBlended with Fe VIII $\lambda 187.241$.

^fPossibly blended with Mn IX $\lambda 188.48$.

^gWavelengths not directly measured by Ekberg (1981), but deduced from other wavelength measurements.

4.1. Lines in the EIS LW band

The Fe VII lines in the LW band consist of decays from two $n = 4$ terms, $3p^63d4s\ ^3D$ and $3p^63d4p\ ^1P$, together with decays from the $3p^53d^3\ ^5S$, 5D and 5F terms. The latter two each give rise to two groups of lines corresponding to decays to the 3P and 3F terms in the ground $3p^63d^2$ configuration. Line ratios formed from the $3p^53d^3$ lines are relatively insensitive with regard density and temperature, and we compare with the strongest line, $\lambda 249.30$, below. There is significant temperature sensitivity when comparing lines from different configurations. We go through the LW lines by multiplet, starting with the longest wavelengths.

Four emission features are found between 289 and 291 Å, at the very end of the EIS wavelength range. These are principally due to the Fe VII $3d^2\ ^3F_J - 3d4s\ ^3D_{J'}$ transitions, which were first identified by Brown et al. (2008) from EIS spectra. The strongest line is a blend of the $J = 4$ to $J' = 3$ and 3–2 transitions, and also has the Si IX $\lambda 290.69$ line in the short wavelength wing. The feature was fit with two Gaussians forced to have the same width, with the short wavelength Gaussian representing the Si IX line. The remaining three emission features are unblended. Each of $\lambda 289.68$, $\lambda 289.83$ and $\lambda 290.31$ shows only weak sensitivity to density and temperature relative to $\lambda 290.72 + \lambda 290.76$, and the comparison with theory is shown in Table 5. $\lambda 290.31$ is discrepant with theory, with the observed line being too strong, however both $\lambda 289.68$ and $\lambda 289.83$ agree with theory within the error bars. Table 2 shows that the measured velocities of $\lambda 289.68$ and $\lambda 289.83$ are discrepant with the standard cool line velocity. The reference wavelengths for the $3d^2\ ^3F_J - 3d4s\ ^3D_{J'}$ transitions given in Paper I are obtained from the energies of Ekberg (1981), who was able to obtain the $3d4s$ level energies indirectly by measuring $4s-4p$ transitions at wavelengths 1000–1400 Å and $3d-4p$ transitions at wavelengths 200–300 Å. Since the EIS wavelengths are direct measurements of the $3d-4s$ transitions then the velocity discrepancies for $\lambda 289.68$ and $\lambda 289.83$ may be due to uncertainties in the Ekberg (1981) $4s$ configuration energies.

The Fe VII model predicts two lines arising from the $3p^53d^3(^4P)\ ^5S_2$ level whose theoretical wavelengths are 270.40 and 271.20 Å, with the latter being stronger by around a factor 3. The spectra were searched in this region for two lines with the same ratio and wavelength separation, and whose images are consistent with a cool line. The lines observed in the atlas at 271.068 and 271.729 Å were found to match and so we identify these with the $3p^53d^3(^4P)\ ^5S_2$ level for which we are thus able to establish an experimental energy value for the first time (Table 3). The longer wavelength line was used to revise the energy since the shorter wavelength line is blended (see below), and a velocity shift of $-40.4\ \text{km s}^{-1}$ was applied to determine the rest wavelengths, as described in the previous section. The rest wavelengths of the two decays from the 5S_2 level are then 271.067 and 271.692 Å for the decays to the 3P_1

and 3P_2 levels in the ground configuration, respectively. $\lambda 271.69$ seems to be unblended and comparing with the strongest line from $3p^5 3d^3$ in the LW band, the $\lambda 271.69/\lambda 249.30$ ratio shows weak sensitivity to density and temperature and the theoretical value agrees well with observations (Table 5). The observed line at 271.068 \AA is a very broad feature, suggesting it is a blend of two or more lines, and Paper I showed that two O V lines contribute, although they can not fully account for the line’s intensity. The Fe VII $\lambda 271.07/\lambda 271.69$ branching ratio is 0.31 and implies that Fe VII contributes an intensity of $7.7 \text{ erg cm}^{-2} \text{ s}^{-1} \text{ sr}^{-1}$ to the blend.

Around $265\text{--}267 \text{ \AA}$ the Fe VII model gives a line with known wavelength at 265.70 \AA , and five lines with theoretical wavelengths due to $3p^6 3d^2 \ ^3P_J - 3p^5 3d^3 (^4F) \ ^5D_{J'}$ transitions. The known line is the only decay from the $3p^6 3d 4p$ configuration found in the EIS spectrum and Table 2 shows the measured wavelength is consistent with the laboratory wavelength of Ekberg (1981). The $\lambda 265.70/(\lambda 290.72 + \lambda 290.76)$ ratio is found to be an excellent temperature diagnostic (Fig. 3), although it also shows some density sensitivity. Taking the Mg VII density of $\log N_e = 9.15$, we find a temperature of $\log T = 5.47^{+0.08}_{-0.07}$, which is close to the expected temperature of formation of Fe VII. Note that $\lambda 265.70$ is blended with a high temperature Co XVI line (Brown et al. 2008), but this makes no contribution in the present spectrum.

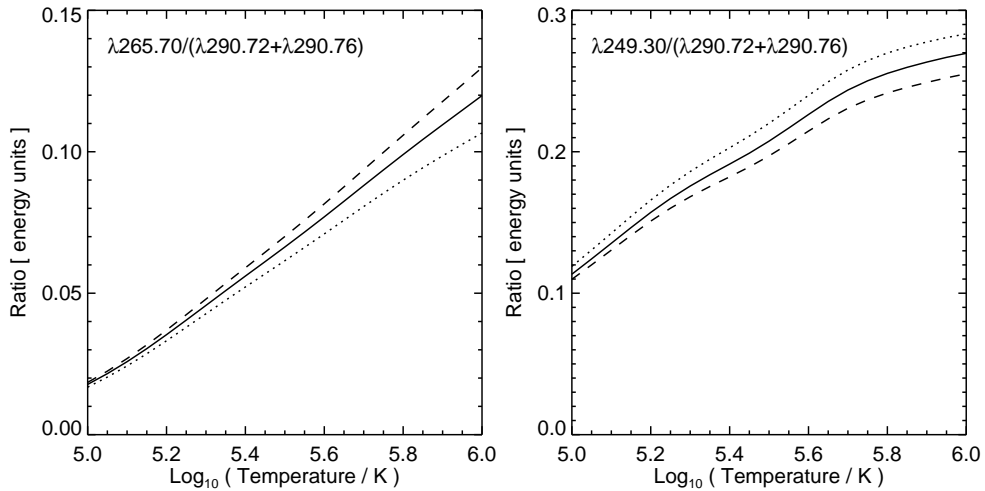


Fig. 3.— Theoretical ratios formed from lines found in the EIS LW band that arise from different configurations. The left panel shows $\lambda 265.70/(\lambda 290.72 + \lambda 290.76)$ and the right shows $\lambda 249.30/(\lambda 290.72 + \lambda 290.76)$. The ratios are plotted as a function of temperature and the different lines correspond to densities of $\log N_e = 8.5$ (dotted), 9.0 (solid) and 9.5 (dashed).

Studying images formed in the weak observed lines between 266 and 267.5 Å, the 267.29 Å line is found to be close in temperature to Fe VII. The line is broad, suggesting it consists of more than one transition, and we note that the 2–2, 2–1 and 2–3 transitions of the $3p^63d^2\ ^3P_J - 3p^53d^3(^4F)\ ^5D_{J'}$ multiplet are predicted to lie within 0.13 Å of each other. Summing the theoretical emissivities of each component and taking the ratio relative to $\lambda 249.30$ we find good agreement between theory and observation (Table 5) suggesting that the observed line is indeed a blend of three Fe VII components.

Of the other observed emission lines between 266 and 266.7 Å we believe that a weak feature at around 266.42 Å (not reported in Paper I) and the line measured at 266.623 Å have some cool component based on inspection of the images formed in the lines. The 1–1 and 1–0 components of the $3p^63d^2\ ^3P_J - 3p^53d^3(^4F)\ ^5D_{J'}$ multiplet are predicted to be blended and to lie 0.7–0.8 Å to the short wavelength side of the earlier mentioned transitions and thus could be responsible for one or both of these emission lines. Brown et al. (2008) reported a Fe XVII transition at 266.42 Å but this will not be significant in the present spectrum. The 266.62 Å line was measured but not identified by Brown et al. (2008), and inspection of the line image suggests a line formed at around 1–1.5 million K in addition to the cool component. Due to the weakness of the two lines and the unknown contribution of blending it is not possible to make a definite identification of either of these observed lines with specific Fe VII transitions.

Our prescription for revising the energy levels for the $^5D_{J'}$ term is to fit the broad line at 267.29 Å with two Gaussians of the same width, giving components at 267.245 and 267.303 Å with intensities 13.7 and 19.8 erg cm⁻² s⁻¹ sr⁻¹ (Paper I). The longer wavelength component is assumed to be the 2–2 transition (which is predicted to have the longest wavelength), yielding an experimental energy for the $3p^53d^3(^4F)\ ^5D_2$ level of 395 436 cm⁻¹. The shorter wavelength measured line is then assumed to be a blend of the 2–1 and 2–3 components. Note that the predicted ratio of the combined 2–1 and 2–3 transitions relative to the 2–2 transition is 0.72 in very good agreement with the measured ratio of 0.69. The 5D_3 energy value is derived using the $3p^63d^2\ ^3F_3 - 3p^53d^3(^4F)\ ^5D_3$ transition later in this section which yields a predicted wavelength for $3p^63d^2\ ^3P_2 - 3p^53d^3(^4F)\ ^5D_3$ consistent with the measured 267.245 Å line. We can then estimate an energy for the 5D_1 level by assuming that the measured wavelength at 267.245 Å corresponds to the $3p^63d^2\ ^3P_2 - 3p^53d^3(^4F)\ ^5D_1$ transition. The derived energy of 395 517 cm⁻¹ is accurate to only around ± 100 cm⁻¹ as the identified line is blended.

Five lines from the $3p^63d^2\ ^3P_J - 3p^53d^3(^4F)\ ^5F_{J'}$ multiplet are potentially observable in the EIS spectrum but experimental wavelengths are not available. They are predicted to lie in the region 257–259 Å and the strongest line belongs to the $J = 2$ to $J' = 3$ transition. Image inspection for two lines at 259.226 and 260.707 Å reveals they are cool lines, close in

temperature to Fe VII and so are possible candidates. The 259.226 Å line has contributions from Cr VII and Al VII although these can not fully account for the strength of the observed line (Paper I). Based on the strength of the Fe VII $\lambda 249.30$ line the $3p^6 3d^2 \ ^3P_2 - 3p^5 3d^3(^4F) \ ^5F_3$ is too strong to be consistent with the remaining intensity of the 259.226 Å line, and so we identify the observed 260.707 Å line with this transition. The new experimental energy for $3p^5 3d^3(^4F) \ ^5F_3$ is given in Table 3 and the rest wavelength of the transition is 260.672 Å. The $\lambda 260.67/\lambda 249.30$ ratio is predicted to be weakly sensitive to density and temperature and the theoretical ratio is given in Table 5, however the observed ratio is around 25 % lower. No other nearby, unidentified emission lines provide a better match in terms of intensity and so we are confident that the 2–3 transition does correspond to the observed 260.71 Å line.

The next strongest line from the multiplet is the 1–2 transition which is predicted to be a factor 0.59 weaker and 0.64 Å shorter in wavelength. Two candidates in the spectrum are the lines at 259.99 and 260.29 Å. Inspecting images of both lines shows they have a cool component in addition to a hotter component. The 259.99 Å line is a known Fe XII transition and this is confirmed by the line image, while the 260.29 Å line appears to be formed around $\log T = 6.0$. Due to the uncertainty in the identification of the 1–2 transition, we are not able to offer an experimental energy for the $(^4F) \ ^5F_2$ level.

A group of four $3p^6 3d^2 \ ^3F_J - 3p^5 3d^3(^4F) \ ^5D_{J'}$ ($J'=2,3,4$) transitions are predicted between 250 and 253 Å and some guidance as to the location of these lines is given by the earlier identification of the $3p^6 3d^2 \ ^3P_2 - 3p^5 3d^3(^4F) \ ^5D_2$ transition. Firstly we note that the strongest line of the $^3F_J - ^5D_{J'}$ multiplet is predicted to be the 4–4 transition. The difference between the observed energy and theoretical energy for the 5D_2 level derived previously is 3195 cm^{-1} . If we assume the 5D_4 level energy is also discrepant by this amount then the predicted wavelength of the 4–4 transition becomes 253.89 Å. The next strongest line from the multiplet is the 3–3 transition which, again using the energy correction from the 5D_2 level, is expected at 253.45 Å. This line is predicted to be a factor 0.46 weaker than the transition from the 5D_4 level. There is a group of five lines close to these predicted wavelengths, the strongest being an Fe VIII line at 253.98 Å (Sect. 5). The best matches with the Fe VII lines are the two lines measured at 253.56 and 254.09 Å. Images formed in both lines are consistent with other Fe VII images, and the measured ratio is close to the predicted ratio (Table 5). In addition the $\lambda 254.06/\lambda 249.30$ ratio is in agreement with theory. The new experimental energies for the 5D_3 and 5D_4 levels are given in Table 3. With four of the five levels of the 5D multiplet now assigned experimental energies, a revised energy for the remaining level, 5D_0 , can be estimated. The average difference between the experimental and theoretical energies for $^5D_{1-4}$ is -3269 cm^{-1} and subtracting this from the 5D_0 theoretical energy gives the value in Table 3. We estimate this value is accurate to around $\pm 200 \text{ cm}^{-1}$.

Two lines of the $3p^63d^2\ ^3F_J - 3p^53d^3(^4F)\ ^5F_{J'}$ multiplet are predicted to lie close to the short wavelength edge of the EIS LW band: the 4–4 transition at 246.17 Å, and the 4–5 transition at 246.69 Å. As for the previously discussed multiplet, these wavelengths can be revised based on the $3p^63d^2\ ^3P_2 - 3p^53d^3(^4F)\ ^5F_3$ transition identified earlier at 260.678 Å. The difference between the experimental and theoretical energies for 5F_3 that this identification implied is 4413 cm^{-1} . Adjusting the theoretical energies for the 5F_4 and 5F_5 levels by the same amount leads to new predicted wavelengths of 248.55 and 249.08 Å. The atomic model predicts that the short wavelength line is a factor 0.58 times weaker than the long wavelength line. Based on this information, we can identify the Fe VII lines with two lines at 248.67 and 249.33 Å whose ratio is 0.49 ± 0.07 and for which the images are consistent with other Fe VII lines. The new experimental energies for the upper levels of the two transitions are given in Table 3, and the rest wavelengths are 248.635 and 249.295 Å. These two identifications mean that three of five levels of the 5F multiplet now have experimental energies, and these can be used to estimate improved energies for the remaining 5F_1 and 5F_2 levels. The average difference between theoretical and observed energies for $^5F_{3-5}$ is -4575 cm^{-1} , and applying this to the $^5F_{1,2}$ theoretical energies yields the energies listed in Table 3. These values should be accurate to around $\pm 200\text{ cm}^{-1}$.

$\lambda 249.30$ is the strongest of the EIS Fe VII emission lines in the LW band arising from the $3p^53d^3$ configuration and the above paragraphs demonstrated that the ratios amongst the $3p^53d^3$ lines are in good agreement with theory – see also Table 5. We now consider ratios of $\lambda 249.30$ against the strongest lines from the $n = 4$ multiplets.

$\lambda 249.30 / (\lambda 290.72 + \lambda 290.76)$ is temperature sensitive while showing relatively weak density sensitivity (Fig. 3). However, the observed ratio of 0.39 ± 0.04 is outside the range of variability of the theoretical ratio, being too high compared to theory by a factor of around two. $\lambda 249.30 / \lambda 265.70$ shows both temperature and density sensitivity, but if we calculate the theoretical ratio for a density of $\log N_e = 9.15$ and temperature of $\log T = 5.6$ we get a value of 2.83, which compares with the observed ratio of 6.07 ± 0.082 . It thus appears that the atomic data from Witthoef & Badnell (2008) over-predicts the strength of the lines from the $n = 4$ configurations compared to the $3p^53d^3$ configuration, based on the EIS measurements.

This completes our survey of the Fe VII lines in the EIS LW waveband based on the new atomic model. We finish by noting that Ekberg (1981) listed eight transitions arising from levels in the $3p^63d4p$ configuration that lie in the LW band. Only one of these, the $3p^63d^2\ ^1S_0 - 3p^63d4p\ ^1P_1$ transition at 265.70 Å, was discussed above as the predicted intensities of the remaining transitions are all too low to be measured by EIS. For example, the strongest of the seven remaining transitions, $3p^63d^2\ ^3P_0 - 3p^63d4p\ ^3D_1$ at 246.86 Å, is predicted to be 0.47 times weaker than $\lambda 265.70$ by the atomic model. However, the instrument effective

area is lower by further factor of 0.26 at the shorter wavelength, making it too weak to be detectable in the present spectrum.

4.2. Lines in the EIS SW band

All the Fe VII lines expected in the EIS SW band are emitted from the $3p^53d^3$ configuration and Ekberg (1981) provided a large number of line identifications based on laboratory spectra. These identifications were determined by searching for emission lines whose spacing indicated that they represented decays from a single upper level to different lower levels in the ground configuration – the lower level energies being well known, and thus the line separations are accurately predicted. Ekberg (1981) also used theoretical calculations of level energies and radiative decay rates to identify the upper levels. We first make general comments about comparisons between the Ekberg (1981) line identifications and the Witthoef & Badnell (2008) atomic model.

The $3p^53d^3$ configuration consists of 110 fine structure levels from 48 spectroscopic terms. There are many duplicate terms (for example there are six 3D terms) and so it is necessary to differentiate them by specifying the parent terms of the $3d^3$ sub-shell. Witthoef & Badnell (2008) did not specify the parent terms, and so they have been derived separately using the AUTOSTRUCTURE atomic code by one of the present authors (P.R. Young). By matching with the level ordering of the $3p^53d^3$ configuration levels of Ekberg (1981) we confirm all of the parent terms listed by Ekberg (1981), except for his $(^2F)^1D_2$ level, which we find to be $(b^2D)^1D_2$. For the levels identified by Ekberg (1981), the Witthoef & Badnell (2008) theoretical energy values are between 13 000 and 23 000 cm^{-1} larger.

When comparing theoretical structure calculations with previously identified energy levels, there is a risk of mismatches due to level mixing. E.g., if 1F_3 and 3D_3 levels are strongly mixed, then the level names become arbitrary and so one author may assign the name “ 1F_3 ” to a level, while another author might assign “ 3D_3 ”. To ensure that the same level identifications are used, it is necessary to study the strengths of the transitions predicted to arise from the levels. To check this in the present case we have gone through each level identified by Ekberg (1981) and compared his measured intensities for each line emitted by the level, and then compared with the predictions from the new atomic model. For all but one level, the strongest line predicted by the model agrees with the strongest line measured by Ekberg (1981). The one exception is the $3p^53d^3(^2F)^3D_2$ level for which the model gives the decay to 3P_1 to be the strongest, whereas Ekberg (1981) finds the decay to 1D_2 to be the strongest. However, the differences are not large and no other nearby level in the model is consistent with the Ekberg (1981) intensities. We are thus confident that all the Ekberg

Table 3. New level energies for Fe VII.

Level	Energy (cm ⁻¹)
$3p^5 3d^3(^4P) ^5S_2$	389 342
$3p^5 3d^3(^4F) ^5D_0$	395 459 ^a
$3p^5 3d^3(^4F) ^5D_1$	395 342 ^a
$3p^5 3d^3(^4F) ^5D_2$	395 436
$3p^5 3d^3(^4F) ^5D_3$	395 496
$3p^5 3d^3(^4F) ^5D_4$	395 954
$3p^5 3d^3(^4F) ^5F_1$	404 507 ^a
$3p^5 3d^3(^4F) ^5F_2$	404 761 ^a
$3p^5 3d^3(^4F) ^5F_3$	404 893
$3p^5 3d^3(^4F) ^5F_4$	404 518
$3p^5 3d^3(^4F) ^5F_5$	404 452
$3p^5 3d^3(a^2D) ^3F_4$	510 158
$3p^5 3d^3(a^2D) ^3F_3$	513 537 ^a
$3p^5 3d^3(a^2D) ^3F_2$	516 029 ^a
$3p^5 3d^3(^2H) ^3G_4$	512 601
$3p^5 3d^3(^2H) ^1H_5$	538 566
$3p^5 3d^3(^2F) ^3D_1$	546 454 ^a
$3p^5 3d^3(^4P) ^3P_0$	559 991 ^a

^aEnergy derived from theoretical level splittings.

(1981) levels are correctly matched with levels of the same name in the Witthoeft & Badnell (2008) model.

In the following paragraphs we will systematically go through each of the eleven spectroscopic terms in the Fe VII $3p^53d^3$ configuration that give rise to the EIS SW lines, starting with the longest wavelength lines. In order to check the consistency of the line intensities we will make three types of comparison: (i) ratios of lines emitted from the same upper level (branching ratios); (ii) ratios relative to the strongest line from a multiplet; and (iii) ratios relative to the strongest line in the EIS SW band, the $3p^63d^2\ ^3F_4 - 3p^53d^3(^2H)\ ^3G_5$ transition, $\lambda 195.39$. Since all of the Fe VII transitions in the EIS SW band are due to $3p^63d^2 - 3p^53d^3$ transitions, we will not refer to configurations in the notation below. Thus, e.g., $^3F_4 - (^2H)^3G_5$ refers to the $3p^63d^2\ ^3F_4 - 3p^53d^3(^2H)\ ^3G_5$ transition.

Working through the Fe VII lines from the longest wavelengths in the SW band through to the shortest, we begin with the two lines from the $(^2F)^3G_3$ level: the decay to 3F_2 at $207.71\ \text{\AA}$ and the decay to 3F_3 at $208.17\ \text{\AA}$. The former is the stronger and the wavelength is consistent with the Ekberg (1981) laboratory measurement (Table 2). Comparing with the strongest Fe VII line seen in the EIS spectrum, $\lambda 195.39$, the $\lambda 207.71/\lambda 195.39$ ratio is found to be relatively insensitive to density and temperature and the measured line ratio is around 25 % larger than predictions (Table 5). The $\lambda 208.17$ line can also be identified in the spectrum and, although very weak, the observed intensity is consistent with the $\lambda 207.71$ line (Table 4), while the derived velocity is also consistent with other cool lines (Table 2).

The strongest line from the $(^2F)^1G_4$ level is the decay to 3F_3 at $201.86\ \text{\AA}$. This line is observed in the EIS spectrum partly in the short wavelength wing of the stronger Fe XIII $\lambda 202.04$ line, and the wavelength is consistent with the Ekberg (1981) laboratory measurement (Table 2). The strength of $\lambda 201.86$ is compared with the strong $\lambda 195.39$ Fe VII line in Table 5, however the observed line is stronger than predictions by a factor 2. A further line from $(^2F)^1G_4$ is the decay to 3F_4 at $202.38\ \text{\AA}$, which is predicted to be a factor 5.0 less than $\lambda 201.86$. In the EIS spectrum at this wavelength there is a feature that can be fit with two Gaussians giving the two lines at 202.344 and $202.420\ \text{\AA}$ in the line list table (Paper I). Neither of these wavelengths is consistent with the Fe VII line. The stronger line at $202.42\ \text{\AA}$ was identified as a blend of Fe XI and Fe XIII by Brown et al. (2008). However the Fe XIII identification is incorrect as the $3s^23p^2\ ^3P_1 - 3s^23p3d\ ^3P_0$ transition actually occurs at $203.16\ \text{\AA}$. An image formed in the $202.42\ \text{\AA}$ line is clearly consistent with Fe XI and there is a suggestion that a cool line contributes at the footpoint regions, but this is not clear. The Fe VII $\lambda 202.38/\lambda 201.86$ branching ratio implies that Fe VII contributes an intensity of $10\ \text{erg cm}^{-2}\ \text{s}^{-1}\ \text{sr}^{-1}$ to the measured line at $202.42\ \text{\AA}$.

The $^3F_J - (^2H)^3G_{J'}$ multiplet is the most important group of Fe VII lines observed by

EIS as they lie very close to the peak sensitivity of the instrument, making them the strongest Fe VII lines. However there are problems reconciling the Ekberg line identifications with the atomic model and the measured EIS line intensities. The situation is complicated by the fact that the model predicts further lines from the ${}^3F-(a^2D){}^3F$ and ${}^1G-({}^2H){}^1H$ multiplets to lie close to the ${}^3F_J - ({}^2H){}^3G_{J'}$ multiplet.

The strongest lines from the ${}^3F_J - ({}^2H){}^3G_{J'}$ multiplet are given by Ekberg at 195.39 Å (4–5), 196.42 Å (3–4), and 196.05 Å (2–3). The atomic model predicts the relative strengths to be 1.0:0.68:0.35. Lines can be seen corresponding to each of the Ekberg lines in the EIS spectra, however their ratios are 1.0:0.20:0.36. The ${}^3F_3 - ({}^2H){}^3G_4$ line is thus clearly discrepant with theory by a factor 3.

In the vicinity of these three lines in the EIS spectra we find two unidentified lines at 195.51 and 196.24 Å whose images are consistent with Fe VII. The measured ratios of these lines relative to 195.40 are 0.52 and 0.51 and are thus more consistent with the predicted intensity of the ${}^3F_3 - ({}^2H){}^3G_4$ transition. The theoretical model of Fe VII predicts that the ${}^3F_3 - ({}^2H){}^3G_4$ transition lies between the wavelengths of ${}^3F_4 - ({}^2H){}^3G_5$ and ${}^3F_2 - ({}^2H){}^3G_3$. We thus believe that the observed line at 195.51 Å is actually the ${}^3F_3 - ({}^2H){}^3G_4$ transition, and we use the measured wavelength to derive a new experimental energy for the $({}^2H){}^3G_4$ level which is given in Table 3. The rest wavelength for the ${}^3F_3 - ({}^2H){}^3G_4$ transition is then 195.480 Å. We stress that there is some uncertainty over this identification on account of the fact that the $\lambda 195.48/\lambda 195.39$ ratio is discrepant with the prediction from the atomic model as shown in Table 5 with $\lambda 195.48$ apparently too weak in observations by around 25 %, however no better solution for the identification of this strong transition can be found.

To explain the decays to 3F_3 and 3F_4 that Ekberg identified with $({}^2H){}^3G_4$, we find that they are consistent with transitions from $(a^2D){}^3F_4$. The theoretical data of Witthoef & Badnell (2008) place $(a^2D){}^3F_4$ very close in energy to the $({}^2H){}^3G$ levels, implying the decays to the 3F ground term will be close in wavelength. In addition the predicted ${}^3F_4 - (a^2D){}^3F_4$ to ${}^3F_3 - (a^2D){}^3F_4$ intensity ratio is 0.44, consistent with Ekberg’s measured ratio of 0.47. (The predicted ${}^3F_4 - ({}^2H){}^3G_4$ to ${}^3F_3 - ({}^2H){}^3G_4$ intensity ratio is 0.04 and so is inconsistent with Ekberg’s measurements.) By making the identification of the $(a^2D){}^3F_4$ level with Ekberg’s transitions we transfer Ekberg’s experimental energy for $({}^2H){}^3G_4$ to $(a^2D){}^3F_4$, and this energy is given in Table 3. No experimental energies were available for the $(a^2D){}^3F_2$ and $(a^2D){}^3F_3$ levels and so we have used the difference between the experimental and theoretical energies for $(a^2D){}^3F_4$ to adjust the theoretical energies for these two levels, and the new values are given in Table 3. With regard the EIS spectra, the $\lambda 196.42$ line that we identify with ${}^3F_3 - (a^2D){}^3F_4$ is partly blended with Fe XIII $\lambda 196.52$ (note the revised wavelength of this transition suggested by Young et al. 2009) as well as another Fe VII line, the

${}^3F_3 - ({}^2H) {}^3G_3$ transition at 196.45 Å. Inspection of the observed feature shows an emission line with an extended shoulder on the long wavelength side, corresponding to dominant Fe VII emission and a weak Fe XIII component. It can be fit with two Gaussians forced to have the same width (Table 4 of Paper I) and the Fe XIII component intensity results in the Fe XIII $\lambda 196.54/\lambda 202.04$ density diagnostic yielding a density of $\log N_e = 9.0$, which is reasonably consistent with the $\lambda 200.02/\lambda 202.04$ ratio of the same ion. If we assume the remaining component of the observed feature comprises the $\lambda 196.42$ and $\lambda 196.45$ transitions then we can estimate the $\lambda 196.45$ contribution as $8.5 \text{ erg cm}^{-2} \text{ s}^{-1} \text{ sr}^{-1}$ (24 %) based on the $\lambda 196.45/\lambda 196.05$ branching ratio which has a value of 0.106. This leaves an estimated intensity of $26.6 \pm 1.4 \text{ erg cm}^{-2} \text{ s}^{-1} \text{ sr}^{-1}$ for $\lambda 196.42$. However, this is a factor two stronger than expected based on the theoretical $\lambda 196.42/\lambda 195.39$ ratio (Table 5).

The strongest transition from the $(a^2D) {}^3F$ term is ${}^3F_2 - (a^2D) {}^3F_3$, and with the theoretical $(a^2D) {}^3F_3$ energy revised as above the predicted wavelength becomes 194.728 Å. The predicted ratio relative to $\lambda 195.39$ is 0.152 ± 0.007 , while that relative to $\lambda 196.42$ is 2.28 ± 0.48 placing the expected intensity somewhere between 34 and 61 $\text{erg cm}^{-2} \text{ s}^{-1} \text{ sr}^{-1}$. A possible candidate is the line measured at 194.82 Å in the present spectrum. Inspecting the image formed from this line suggests that it is mostly due to Fe IX (see Sect. 6), however by forming an image towards the short wavelength side of the line, a cool component similar to Fe VII can be seen. The line at 194.82 Å is broader than the nearby Fe VIII $\lambda 194.66$ and Fe IX $\lambda 197.86$ lines suggesting that it is a blend of two lines, and the measured intensity of the line is consistent with it partly consisting of the Fe VII ${}^3F_2 - (a^2D) {}^3F_3$ transition. Despite this we do not make a definite identification of the Fe VII transition with the observed line and so do not revise the $(a^2D) {}^3F_3$ energy. Analysis of high resolution laboratory spectra may possibly be able to confirm the identification.

Returning to the ${}^3F_J - ({}^2H) {}^3G_{J'}$ multiplet, we note that the image formed in the $\lambda 195.39$ line shows a contribution from a coronal line which is consistent with Fe X. Bromage et al. (1977) identified the Fe X $3s^2 3p^5 {}^2P_{3/2} - 3s^2 3p^4 ({}^1S) 3d^2 D_{3/2}$ transition with a line at 195.399 Å in laboratory spectra, however Keenan et al. (2008) identified the transition with a line at 195.32 Å in solar spectra. Based on several different spectra taken with EIS, Brown et al. (2008) identify the Fe X transition with the laboratory wavelength, and find no line corresponding with the line observed by Keenan et al. (2008). For this work we have inspected a quiet Sun off-limb spectrum (where Fe VII is negligible) and confirm that the Fe X wavelength is 195.40 Å. Note that the Fe X model in CHIANTI does not give an observed wavelength for the transition, instead the theoretical wavelength of 195.316 Å is used – see Del Zanna et al. (2004). We can use the CHIANTI model to estimate the contribution of Fe X to the Fe VII $\lambda 195.39$ line: Fe X $\lambda 195.40/\lambda 184.54$ is found from CHIANTI to be density sensitive, ranging from 0.025 at $\log N_e = 8$ to 0.057 at $\log N_e = 12$. If we use the density derived from Mg VII

of $\log N_e = 9.15$, then the predicted Fe X ratio is 0.032. The measured Fe X $\lambda 184.54$ intensity is $504.3 \text{ erg cm}^{-2} \text{ s}^{-1} \text{ sr}^{-1}$, giving a predicted Fe X $\lambda 195.40$ intensity of $16 \text{ erg cm}^{-2} \text{ s}^{-1} \text{ sr}^{-1}$ – only a 7 % contribution to the measured line at 195.42 \AA .

The Fe VII $^3F_3 - (^2H)^3G_4$ transition, $\lambda 195.48$, lies close to the Ni XV $3s^23p^2 \ ^1D_2 - 3s^23p3d \ ^1D_2$ transition at 195.52 \AA (Brown et al. 2008), but this line is negligible in the present spectrum as it is formed at $\log T = 6.4$. The $^3F_2 - (^2H)^3G_3$ transition, $\lambda 196.05$, lies in the long wavelength wing of the stronger Fe VIII $\lambda 195.97$ line, and a two Gaussian fit is necessary to separate the components. Brown et al. (2008) list a O IV transition between the Fe VIII and Fe VII lines, but there is no evidence for this line here.

The $^1G_4 - (^2H)^1H_5$ transition is predicted by the atomic model to be 0.53 times the intensity of the $^3F_4 - (^2H)^3G_5$ transition at 195.39 \AA , and the theoretical wavelength is 1.06 \AA longward of this transition. Therefore the observed line at 196.24 \AA is an excellent match. The only other line predicted to arise from the $(^2H)^1H_5$ level in the EUV is the decay to 3F_4 which occurs around 10 \AA shorter in wavelength compared to the decay to 1G_4 . The atomic model predicts this line to be 43 times weaker and so it can not be observed by EIS. The measured wavelength of the 196.24 \AA line is used to derive a new energy value for the $(^2H)^1H_5$ level, and this is given in Table 3. The rest wavelength of the transition is then 196.217 \AA . Note that $\lambda 196.22/\lambda 195.39$ is a good density diagnostic and Fig. 4 shows the variation with density at three temperatures. For the present spectrum, choosing the temperature of $\log T = 5.55$ we find a density of $\log N_e = 8.68 \pm 0.08$, which is significantly lower than the values from the Mg VII and Si VII density diagnostics (Paper I). To obtain the Mg VII density, the observed $\lambda 196.22/\lambda 195.39$ ratio would have to be increased by only 10 % which is a relatively small discrepancy compared to other ratios discussed in this section.

The $(a^2D)^1D_2$ level gives rise to only one line capable of being seen by EIS: the decay to 1D_2 at wavelength 192.006 \AA . This line is blended with Fe VIII $\lambda 192.01$ and a coronal line, which we believe to be due to Fe XI. The Fe VII $\lambda 192.01/\lambda 195.39$ ratio is weakly sensitive to density and temperature with a value of 0.041 ± 0.007 , and so the Fe VII contribution to the 192.01 \AA line can be estimated as $9.2 \pm 2.5 \text{ erg cm}^{-2} \text{ s}^{-1} \text{ sr}^{-1}$ (12 % of the total line intensity), using the measured $\lambda 195.39$ intensity. In Sect. 5 the Fe VIII contribution to the observed 192.02 \AA line is estimated to be 54 %.

Ekberg (1981) identified lines from the $J = 2$ and $J = 3$ components of the $(^2F)^3D_J$ multiplet, but not from the $J = 1$ component. We discuss first the identified lines. The strongest line predicted by the atomic model is the $^3P_2 - (^2F)^3D_3$ transition at 188.58 \AA which lies in the wing of the stronger Fe IX $\lambda 188.50$ line. A simultaneous 15 Gaussian fit was performed over the range 187.71 to 189.13 \AA due to the lack of nearby continuum around these lines. The Fe VII line is found to be much weaker than expected: $\lambda 188.58/\lambda 195.39$

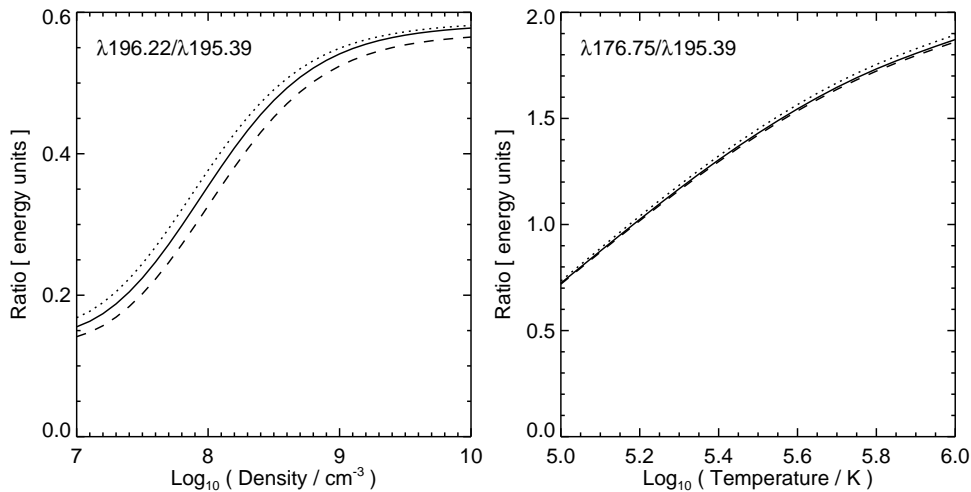


Fig. 4.— Theoretical ratios formed from lines found in the EIS SW. The left panel shows the density sensitive $\lambda 196.22/\lambda 195.39$ ratio, with curves calculated at temperatures of $\log T = 5.40$ (dotted line), 5.55 (solid line) and 5.70 (dashed line). The right panel shows the temperature sensitive $\lambda 176.75/\lambda 195.39$ ratio, with curves calculated at densities of $\log N_e = 8.5$ (dotted), 9.0 (solid) and 9.5 (dashed).

has a theoretical value of 0.489 ± 0.068 , yet the observed ratio is 0.253 ± 0.034 . The next strongest line from the $(^2F)^3D_3$ level is the decay to 1D_2 at 187.24 \AA which is blended with Fe VIII $\lambda 187.24$ and, as noted in Sect. 5, Fe VII appears to contribute more than half of the measured intensity. This actually makes it a little stronger than $\lambda 188.58$ whereas theory predicts it to be almost a factor four weaker. A further line emitted from the $(^2F)^3D_3$ level is the decay to 3F_4 at 182.07 \AA . Although predicted to be only 0.13 the strength of $\lambda 188.58$, a line can be identified in the wing of Fe XI $\lambda 182.16$ that appears to be the Fe VII transition. The line fit parameters in the line list table of Paper I are derived by forcing the Fe VII line to have the EIS instrumental width of 56 m\AA , otherwise an unrealistically narrow line results. The line velocity is consistent with the other Fe VII transitions (Table 2), but the $\lambda 182.07/\lambda 188.58$ ratio of 0.407 ± 0.164 is significantly discrepant with theory. These results suggest that the atomic data for the $(^2F)^3D_3$ level are in error.

The strongest line predicted from the $(^2F)^3D_2$ level is at 189.45 \AA and this can be identified in the EIS spectrum. Comparing with the strongest line from the $(^2F)^3D_3$ level, the $\lambda 189.45/\lambda 188.58$ ratio shows weak sensitivity to density and temperature but the observed ratio is almost a factor two stronger than the predicted ratio (Table 5). This is consistent with the problems discussed in the previous paragraph with regard the $(^2F)^3D_3$ level, and we note that $\lambda 189.45/\lambda 195.39$ is in better agreement with theory (Table 5). The next strongest

line predicted from $(^2F)^3D_2$ is the decay to 1D_2 at 188.40 Å which, however, is observed to be stronger than $\lambda 189.45$: the observed $\lambda 188.40/\lambda 189.45$ branching ratio is almost a factor two larger than the predicted value (Table 5). Table 4 in Paper I lists a Mn IX transition as a possible blend to $\lambda 188.40$, contributing 30 % to the observed line intensity based on the DEM intensity prediction. As mentioned in Paper I, the experimental wavelength of the Mn IX line is only accurate to ± 0.05 Å and so it could actually be blending with the nearby Fe IX $\lambda 188.50$ line, but the large Fe VII branching ratio discrepancy suggests it is more likely to blend with Fe VII $\lambda 188.40$. A decay to the level 3F_3 gives a line at 182.74 Å which is seen in the EIS spectra, although the wavelength shows a small discrepancy compared to the Ekberg (1981) laboratory wavelength (Table 2). The $\lambda 182.74/\lambda 189.45$ branching ratio is consistent with theory (Table 5), however. A further decay to 3P_2 is predicted at 189.76 Å, with the $\lambda 189.76/\lambda 189.45$ branching ratio suggesting an intensity of around $9 \text{ erg cm}^{-2} \text{ s}^{-1} \text{ sr}^{-1}$. A line at this wavelength can not be clearly seen in the spectrum, however.

Ekberg (1981) did not report any lines from the $(^2F)^3D_1$ level, however the atomic model predicts three potentially observable lines. The Witthoeft & Badnell (2008) atomic data yield predicted wavelengths for these lines, but more accurate predicted wavelengths can be obtained by making use of the experimental energies of the $(^2F)^3D_{2,3}$ levels. We first note that the Witthoeft & Badnell (2008) theoretical energy for $(^2F)^3D_1$ is $568\,459 \text{ cm}^{-1}$, while the average difference between the theoretical and observed energies for $(^2F)^3D_{2,3}$ is $+22\,006 \text{ cm}^{-1}$. We thus estimate a revised energy for $(^2F)^3D_1$ of $546\,454 \text{ cm}^{-1}$ which has an accuracy of around $\pm 2\,000 \text{ cm}^{-1}$. The strongest line emitted by $(^2F)^3D_1$ is the decay to 3P_0 with a predicted wavelength of 189.97 Å which is accurate to around ± 0.7 Å. It is insensitive relative to the strongest line from $(^2F)^3D_2$ ($\lambda 189.45$) with a value 0.508 ± 0.040 , which makes it a good match for the line observed at 189.36 Å: the observed ratio being 0.574 ± 0.039 . Images formed in the 189.36 Å line are also consistent with Fe VII. If this identification is correct then we also expect two further lines at 182.436 and 189.499 Å in the spectrum whose ratios relative to the stronger line are 0.43 and 0.68, respectively. There is a weak line seen at 182.430 Å however the ratio relative to the 189.36 Å line is 0.708 ± 0.185 , and so higher than theory predicts. If a line exists at 189.499 Å it will partly blend with the observed Fe VII line at 189.481 Å. The line width of the latter is not anomalously broad and so the predicted line at 189.499 Å is either not there, or anomalously weak. Because of these problems we do not identify the observed 189.359 Å line with the Fe VII $^3P_0 - (^2F)^3D_1$ transition.

The strongest transition predicted from the $(b^2D)^1D_2$ level is the decay to 1D_2 at 186.66 Å, which places it in the wing of the strong Fe VIII $\lambda 186.60$ line. Performing a two Gaussian fit to $\lambda 186.60$ reveals a weak line in the long wavelength wing, however the wavelength is longer than expected based on the reference Fe VIII lines (Table 2). Brown et al.

(2008) identified the line at this wavelength as a Ni XIV transition, however the intensity predicted for this line using the DEM is $< 1 \text{ erg cm}^{-2} \text{ s}^{-1} \text{ sr}^{-1}$ and so it can be ignored in the present case. If we assume that Fe VII accounts entirely for the measured line, then the discrepant wavelength suggests that the two Gaussian fit may not be accurately measuring the weak line. This is also suggested by a look at the $\lambda 186.66/\lambda 195.39$ ratio, which is weakly sensitive to temperature and density: Table 5 shows that $\lambda 186.66$ is weaker than expected by more than a factor two. Two further lines are predicted to arise from the $(b^2D)^1D_2$ level: the decays to the $^3P_{1,2}$ ground levels at wavelengths 187.69 and 187.99 Å, respectively, and the branching ratios are 0.13 and 0.11. Based on the measured intensity of $\lambda 186.66$ the lines should be very weak, but a line is observed at 187.71 Å that is consistent with the expected position of $\lambda 187.69$ (Table 2) and for which the image is consistent with Fe VII. The observed intensity, however, is much stronger than expected (Table 4), with the measured line at 187.71 Å almost half the strength of $\lambda 186.66$. A line is observed at 187.972 Å but we believe this is a Fe IX transition (Sect. 6). Fe VII $\lambda 187.99$ will lie in the long wavelength wing of the this line, but no significant feature is found here implying the line is weak.

The $(^2G)^1F_3$ level gives rise to two lines at 185.55 Å and 186.87 Å, and the branching ratio $\lambda 186.87/\lambda 185.55$ is 0.218. Lines at both wavelengths are observed, but $\lambda 186.87$ is blended with a Fe XII feature that is itself a blend of two lines at 186.85 and 186.89 Å. Assuming $\lambda 185.55$ is unblended, Fe VII is predicted to contribute $14.4 \pm 0.9 \text{ erg cm}^{-2} \text{ s}^{-1} \text{ sr}^{-1}$ (8 %) to the measured feature at 186.88 Å. $\lambda 185.55/\lambda 195.39$ is relatively insensitive to density and temperature, but the observed ratio is around 40 % below the predicted value (Table 5).

Ekberg (1981) identified emission lines from the $J = 1$ and $J = 2$ components of the $(^4P)^3P_J$ term, but for the $J = 0$ component only one line is predicted by the atomic model – the decay to 3P_1 – and so Ekberg’s method of identifying multiple lines from a single level can not be applied. An improved estimate of the $^3P_1 - (^4P)^3P_0$ wavelength can be made, however, by taking the average energy difference between the observed and theoretical energies for the $(^4P)^3P_{1,2}$ levels, and applying this to the theoretical energy of $(^4P)^3P_0$. The resulting energy is given in Table 3 and we estimate has an accuracy of around $\pm 500 \text{ cm}^{-1}$. The predicted wavelength for $^3P_1 - (^4P)^3P_0$ is then 185.34 Å with an accuracy of around ± 0.2 Å. This line is insensitive relative to the strongest line from the $(^4P)^3P_J$ term, $\lambda 183.83$, with a theoretical value of 0.250 ± 0.024 , and so should have an intensity around $23 \text{ erg cm}^{-2} \text{ s}^{-1} \text{ sr}^{-1}$. No obvious candidate in the EIS spectrum can be found, but possibly it is blended with the strong Fe VIII $\lambda 185.21$ line.

The $(^4P)^3P_1$ level gives rise to three lines of comparable strength at wavelengths 184.75, 184.89 and 185.18 Å, corresponding to decays to the $^3P_{0,1,2}$ levels in the ground configuration.

They are each predicted to be around one quarter of the strength of the ${}^3P_2 - ({}^4P) {}^3P_2$ transition at 183.83 Å. $\lambda 185.18$ is blended with the strong Fe VIII $\lambda 185.21$ line and makes a $< 2\%$ contribution. Table 4 of Paper I indicates that $\lambda 184.89$ is blended with Ne VI, although it was noted that the measured wavelength is not consistent with the Ne VI wavelength. If the measured intensity is assumed to be entirely due to Fe VII then $\lambda 184.89/\lambda 183.83$ is in good agreement with theory (Table 5). The measured wavelength, however, shows a discrepancy of around 20 km s^{-1} (Table 2). The image formed in the line is consistent with the formation temperatures of both Ne VI and Fe VII. Table 4 in Paper I also indicates that Fe VII $\lambda 184.75$ is blended with Fe XI and Ne V, and based on the measured Fe VII $\lambda 183.83$ line intensity Fe VII would be expected to contribute around 60%. However, the DEM predictions for Ne V and Fe XI account for 80% of the measured intensity. No other Ne V line is found in the spectrum so an independent check of the line’s intensity is not possible (Paper I), while the Fe XI line is strongly density dependent relative to other Fe XI lines such as $\lambda 188.23$ so the predicted contribution depends critically on the density chosen for the DEM analysis. We note that the measured wavelength of the $\lambda 184.777$ Å line is consistent with Fe VII $\lambda 184.75$ (Table 2). The image formed in the $\lambda 184.75$ line clearly reveals a blend with a coronal line with temperature around that of Fe XI, however a cool component can also be seen.

Two potentially observable lines are predicted from the $({}^4P) {}^3P_2$ level: the decay to 3P_1 at 183.54 Å and the decay to 3P_2 at 183.83 Å. Lines at both wavelengths are found, but the observed $\lambda 183.54/\lambda 183.83$ ratio is a factor 2 lower than theory (Table 5). The $\lambda 183.83/\lambda 195.39$ ratio is relatively insensitive to density and temperature, and theory agrees well with observation (Table 5).

The shortest wavelength Fe VII lines observed by EIS are the ${}^3F_J - ({}^4F) {}^3F_{J'}$ transitions, and the 4–4 transition at 176.75 Å is in fact the strongest of all the Fe VII lines predicted by the atomic model for typical coronal conditions. The low effective area at this wavelength means the line is rather weak in the EIS spectrum, but it appears to be unblended. The $\lambda 176.75/\lambda 195.39$ ratio is weakly sensitive to density but does show temperature sensitivity as shown in Fig. 4. Using the density of $\log N_e = 9.15$ derived from Mg VII $\lambda 280.72/\lambda 278.39$ (Paper 1) we find a temperature of $\log T = 5.07 \pm 0.10$, much lower than the formation temperature of the ion. To yield a temperature of $\log T = 5.6$ (which we believe to be the T_{max} of the ion) would require an observed ratio of 1.55. Therefore the actual observed ratio is around a factor two lower than expected.

Two additional lines from the ${}^3F_J - ({}^4F) {}^3F_{J'}$ multiplet are predicted to be observed – the 3–3 transition at 176.93 Å and the 2–2 transition at 177.17 Å – but both are blended with stronger lines from other species. $\lambda 176.93$ is blended with a stronger Fe IX line (Sect. 6) and we estimate the Fe VII contribution to be $132.8 \pm 28.1 \text{ erg cm}^{-2} \text{ s}^{-1} \text{ sr}^{-1}$ as the $\lambda 176.75/\lambda 176.93$

ratio has weak sensitivity to density and temperature with a theoretical value of 0.712 ± 0.085 . We note that the measured line is broad, consistent with a blend of two lines with slightly different wavelengths. $\lambda 177.17$ is blended with Fe X $\lambda 177.24$ and, using the $\lambda 177.17/\lambda 176.75$ theoretical ratio of 0.505 ± 0.045 we estimate a Fe VII contribution of $94.2 \pm 18.4 \text{ erg cm}^{-2} \text{ s}^{-1} \text{ sr}^{-1}$.

Finally, we finish this section by comparing lines from the two EIS wavelength bands. The strongest lines emitted by the $3p^5 3d^3$ configuration in the two bands are $\lambda 195.39$ and $\lambda 249.30$. Their ratio is weakly sensitive to density, but strongly temperature sensitive (Fig. 5) and the measured ratio gives a temperature of $\log T = 5.37^{+0.04}_{-0.02}$ which is close to the T_{\max} value given by Bryans et al. (2009) but less than the temperature where we believe Fe VII is actually formed at. For the ratio to yield higher temperatures, the measured $\lambda 249.30$ intensity would have to be weaker than what is actually observed. Comparing $\lambda 195.39$ with the $\lambda 290.72 + \lambda 290.76$ self-blend that arises from the $3p^6 3d4s$ configuration, the ratio is again temperature sensitive, yielding a temperature of $\log T = 5.63 \pm 0.02$ which is more consistent with the apparent formation temperature of Fe VII.

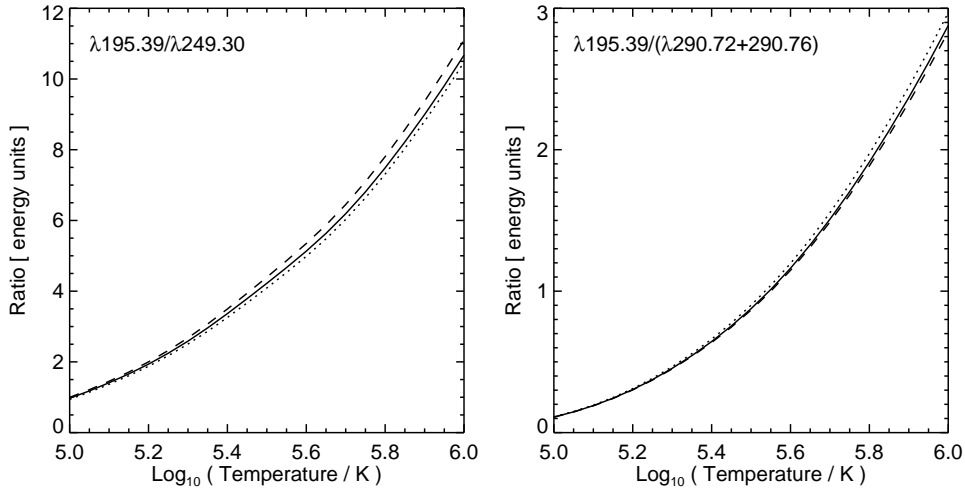


Fig. 5.— Theoretical ratios formed from lines found in the two EIS wavelength bands. The left panel shows $\lambda 195.39/\lambda 249.30$ and the right shows $\lambda 195.39/(\lambda 290.72 + \lambda 290.76)$. The ratios are plotted as a function of temperature and the different lines correspond to densities of $\log N_e = 8.5$ (dotted), 9.0 (solid) and 9.5 (dashed).

Table 4. Fe VII branching ratios.

Upper level	Ratio	Theory	Observation ^a
$3p^5 3d^3(^4P) ^3P_2$	$\lambda 183.54/\lambda 183.83$	0.269	0.132 ± 0.032 ◀
$3p^5 3d^3(^4P) ^3P_1$	$\lambda 184.75^b/\lambda 184.89$	1.07	1.80 ± 0.29
$3p^5 3d^3(b^2D) ^1D_2$	$\lambda 187.69/\lambda 186.66$	0.127	0.459 ± 0.086 ◀
$3p^5 3d^3(^2F) ^3D_3$	$\lambda 182.07/\lambda 188.58$	0.129	0.407 ± 0.164 ◁
	$\lambda 187.23/\lambda 188.58$	0.247	1.095 ± 0.162^c ◀
$3p^5 3d^3(^2F) ^3D_2$	$\lambda 182.74/\lambda 189.45$	0.172	0.202 ± 0.068
	$\lambda 188.40/\lambda 189.45$	0.643	1.26 ± 0.15 ◀
$3p^5 3d^3(^2F) ^3G_3$	$\lambda 208.17/\lambda 207.71$	0.141	0.109 ± 0.063

^aA ◁ symbol indicates that the observed ratio is discrepant with theory by $> 1\sigma$; a ◀ indicates a discrepancy of $> 2\sigma$.

^bBlended with Ne v $\lambda 184.735$ and Fe xi $\lambda 184.803$.

^cThe Fe viii contribution to $\lambda 187.23$ has been subtracted.

Table 5. Fe VII insensitive ratios.

Term ^a	Ratio	Theory	Observation ^b
$3p^5 3d^3(^4P) ^3P$	$\lambda 184.89^c / \lambda 183.83$	0.238 ± 0.007	0.222 ± 0.034
	$\lambda 183.83 / \lambda 195.39$	0.437 ± 0.065	0.404 ± 0.025
$3p^5 3d^3(^2G) ^1F$	$\lambda 185.55 / \lambda 195.39$	0.478 ± 0.078	$0.294 \pm 0.018 \blacktriangleleft$
$3p^5 3d^3(b^2D) ^1D$	$\lambda 186.66 / \lambda 195.39$	0.458 ± 0.069	$0.195 \pm 0.032 \blacktriangleleft$
$3p^5 3d^3(^2F) ^3D$	$\lambda 189.45 / \lambda 188.58$	0.542 ± 0.028	$0.935 \pm 0.129 \blacktriangleleft$
	$\lambda 189.45 / \lambda 195.39$	0.265 ± 0.024	$0.236 \pm 0.010 \triangleleft$
	$\lambda 188.58 / \lambda 195.39$	0.489 ± 0.068	$0.253 \pm 0.034 \blacktriangleleft$
$3p^5 3d^3(^2H) ^3G$	$\lambda 195.48 / \lambda 195.39$	0.698 ± 0.057	$0.520 \pm 0.013 \blacktriangleleft$
	$\lambda 196.05 / \lambda 195.39$	0.359 ± 0.026	0.358 ± 0.013
$3p^5 3d^3(a^2D) ^3F$	$\lambda 196.42 / \lambda 195.39$	0.067 ± 0.015	$0.118 \pm 0.006^d \blacktriangleleft$
$3p^5 3d^3(^2F) ^1G$	$\lambda 201.86 / \lambda 195.39$	0.085 ± 0.017	$0.212 \pm 0.013 \blacktriangleleft$
$3p^5 3d^3(^2F) ^3G$	$\lambda 207.71 / \lambda 195.39$	0.319 ± 0.034	$0.397 \pm 0.036 \triangleleft$
$3p^5 3d^3(^4F) ^5F$	$\lambda 248.64 / \lambda 249.30$	0.593 ± 0.06	0.493 ± 0.067
	$\lambda 260.67 / \lambda 249.30$	0.373 ± 0.032	$0.281 \pm 0.035 \triangleleft$
$3p^5 3d^3(^4F) ^5D$	$\lambda 253.52 / \lambda 254.05$	0.457 ± 0.016	0.385 ± 0.065
	$\lambda 254.05 / \lambda 249.30$	0.800 ± 0.105	0.702 ± 0.085
	$(\lambda 267.21 + \lambda 267.22 + \lambda 267.27) / \lambda 249.30$	0.516 ± 0.050	0.483 ± 0.046
	$(\lambda 267.21 + \lambda 267.22 + \lambda 267.27) / \lambda 254.06$	0.645 ± 0.021	0.688 ± 0.075
$3p^5 3d^3(^4P) ^5S$	$\lambda 271.69 / \lambda 249.30$	0.375 ± 0.053	0.351 ± 0.036
$3p^6 3d 4s ^3D$	$\lambda 289.68 / (\lambda 290.72 + \lambda 290.76)$	0.193 ± 0.001	0.213 ± 0.032
	$\lambda 289.83 / (\lambda 290.72 + \lambda 290.76)$	0.191 ± 0.002	0.205 ± 0.029
	$\lambda 290.31 / (\lambda 290.72 + \lambda 290.76)$	0.267 ± 0.005	$0.389 \pm 0.041 \blacktriangleleft$

^aRatios are grouped according to the spectroscopic term of the upper emitting level. Ratios are formed either between lines emitted from the same term, or one of these lines relative to a reference line ($\lambda 195.39$ for the EIS SW band, and $\lambda 249.30$ for the LW band).

^bA \triangleleft symbol indicates a $> 1\sigma$ discrepancy between theory and observation, \blacktriangleleft indicates a $> 2\sigma$ discrepancy.

^cPossibly blended with Ne VI $\lambda 184.95$.

^dThe contribution of Fe VII $\lambda 196.45$ has been subtracted (see text for details).

4.3. Summary of Fe VII results

The survey of the Fe VII lines in the previous sections have revealed a number of new line identifications in both the SW and LW bands of EIS. The atomic model constructed from the Witthoeft & Badnell (2008) data for CHIANTI yields several line ratios that are good diagnostics of temperature or density. Comparing theory with the EIS observations shows many areas where good agreement is found, but also a number of significant problems. To summarise briefly the main points:

- The ratio of lines from the $3d4p$ and $3d4s$ configurations, $\lambda 265.70/(\lambda 290.72 + \lambda 290.76)$, is a temperature diagnostic.
- Within the LW band (246–291 Å) the atomic model over-predicts the strength of the lines from the $3d4p$ and $3d4s$ configurations compared to the lines from the $3p^53d^3$ configuration by a factor of around two.
- $\lambda 195.39/(\lambda 290.72 + \lambda 290.76)$ is a temperature diagnostic and the derived temperature is close to the expected value for Fe VII.
- Comparing strongest lines from the eleven $3p^53d^3$ spectroscopic terms in the SW band:
 - lines from $(^2F)^3G$, $(^2H)^1H$, $(^2F)^3D_2$ and $(^4P)^3P$ are generally consistent with the $\lambda 195.39$ reference line;
 - lines from $(^2F)^3D_3$, $(b^2D)^1D$, $(^2G)^1F$ and $(^4F)^3F$ are too weak relative to $\lambda 195.39$ by around a factor two;
 - lines from $(^2F)^1G$ are too strong relative to $\lambda 195.39$ by around a factor two.
- $\lambda 196.22/\lambda 195.39$ is identified as a density diagnostic over $\log N_e = 7.0$ to 9.0 , but the derived density here is lower than found from other ions formed at a similar temperature.
- $\lambda 176.75/\lambda 195.39$ is a temperature diagnostic, but the EIS intensities yield a very low temperature, suggesting the atomic model over-predicts the strength of $\lambda 176.75$ relative to $\lambda 195.39$ by a factor of around two.

The good agreement between the measured EIS wavelengths and the Ekberg (1981) reference wavelengths gives confidence in the Ekberg (1981) transition identifications, however the large line ratio discrepancies suggest problems with the current Fe VII atomic data. A new study of high resolution laboratory spectra would be extremely valuable for investigating the problems further. In particular it is important to confirm some of the new and suggested

line identifications found in the present work, for example the 195.48 and 196.21 Å lines and the lines between 248 and 272 Å that arise from the $3p^53d^3$ configuration.

5. Fe VIII

The ground configuration of Fe VIII has only two energy levels, $^2D_{3/2,5/2}$, and the EUV spectrum in the range 160 to 260 Å consists principally of decays from the levels in the $3p^53d^2$ configuration to this ground term. Line identifications are known for all lines between 160 and 200 Å, but for 200–260 Å there are a large number of transitions that are unidentified. The EIS instrument observes the wavelength ranges 170–212 and 246–292 Å and so some of these transitions can be found, but we first focus on the known transitions.

The three terms $3p^53d^2(^3F) ^2F$, $3p^64d ^2P$ and $3p^53d^2(^1S) ^2P$ give rise to nine lines between 185 and 198 Å, all of which are observed in the present spectrum. Reference wavelengths for these lines are available from Ramonas & Ryabtsev (1980), and Table 6 shows the velocities derived from the EIS spectrum using these rest wavelengths. The error bars are derived from the measured centroid uncertainties (Paper I), the estimated uncertainty of ± 0.002 Å in the EIS wavelength scale (Brown et al. 2007), and the uncertainties in the measured wavelengths of Ramonas & Ryabtsev (1980) of ± 0.003 Å. The velocities of the lines unaffected by blending are all less than the typical cool line velocity of $+40.4$ km s $^{-1}$ (Sect. 3), with an average of $+33.0$ km s $^{-1}$. Paper I noted that ions formed above $\log T = 5.8$ showed smaller velocity shifts of around $+20$ km s $^{-1}$ thus the Fe VIII velocities could indicate that it is intermediate between the cool ion and hot ion populations.

Fe VIII line ratios formed from the nine lines between 185 and 198 Å show very little density sensitivity above 10^9 cm $^{-3}$ as the two ground levels are in a quasi-Boltzmann equilibrium above this value. For this reason the lines are little value as density diagnostics in typical coronal conditions. Temperature sensitivity is also weak for these lines. Below 10^9 cm $^{-3}$ significant density sensitivity sets in and this is highlighted for the three strongest Fe VIII lines observed by EIS in Fig. 6. These ratios may be of value in coronal hole or off-limb regions where the density is low, however, the present spectrum reveals some anomalies. The observed $\lambda 185.21/\lambda 186.60$ ratio is found to be 1.28 ± 0.02 which yields a density of $\log N_e = 8.16 \pm 0.05$, significantly below that found from Mg VII in Paper I. There are high temperature blends for both lines (Young et al. 2007a), but both are negligible in the present spectrum. Since the observed ratio is only 14 % below the high density limit of the ratio we believe the discrepancy is most likely due to atomic data uncertainties. $\lambda 194.66/\lambda 186.60$ shows some temperature sensitivity in addition to density sensitivity, however, the measured ratio is 0.402 ± 0.006 , significantly above the range of sensitivity of the ratio. Since the two

Table 6. Fe VIII velocities.

Wavelength (Å)	Velocity (km s ⁻¹)
185.213	30.7 ± 5.8
186.601	36.9 ± 5.8
187.237 ^a	43.2 ± 7.5
192.004 ^b	34.4 ± 7.3
193.967	32.5 ± 6.4
194.662	27.7 ± 5.6
195.972	32.1 ± 5.5
196.650 ^c	21.4 ± 5.6
197.362	38.0 ± 5.5

^aBlended with Fe VII
λ187.235.

^bBlended with Fe VII
λ192.006 and an unknown
hotter line.

^cBlended with Fe XII
λ196.640.

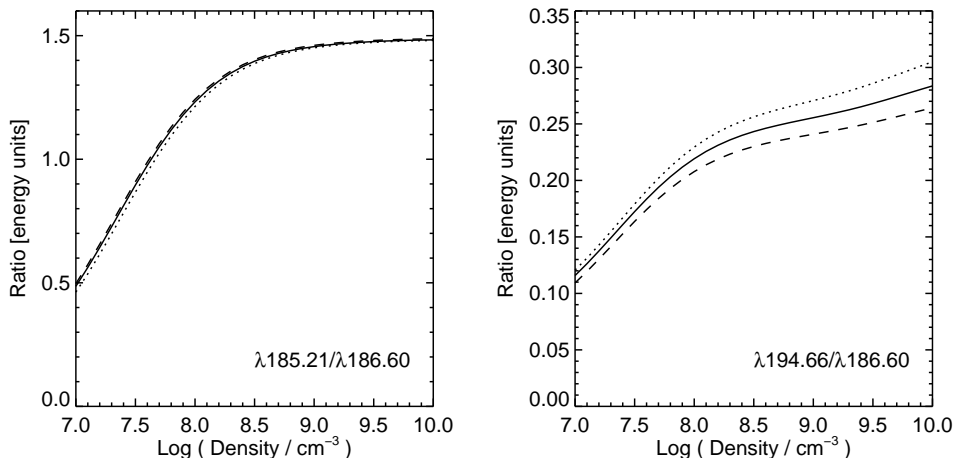


Fig. 6.— Fe VIII emission line ratios showing density sensitivity. The dotted, solid and dashed lines have been calculated for temperatures $\log T = 5.7, 5.8$ and 5.9 , respectively. The left panel shows the $\lambda 185.21/\lambda 186.60$ ratio and the right panel the $\lambda 194.66/\lambda 186.60$ ratio.

lines are both strong and unblended this, again, we believe is due to inaccurate atomic data.

More generally we can investigate atomic data issues through studies of insensitive line ratios. We divide the ratios into Groups 1, 2 and 3 which give an indication of the expected accuracy of the atomic data. Group 1 consists of branching ratios, Group 2 consists of insensitive ratios formed from lines belonging to the same multiplet, while Group 3 consists of insensitive ratios formed from lines belonging to different multiplets. Table 7 presents a comparison between the observed ratios and theoretical ratios calculated with CHIANTI. The atomic model for Fe VIII in CHIANTI consists principally of the electron collision data and radiative decay rates of Griffin et al. (2000), supplemented with additional data from Czyzak & Krueger (1966) and decay rates calculated by the CHIANTI team (Dere et al. 2001).

None of the Group 1 measured ratios agrees with theory, although $\lambda 193.97/\lambda 194.66$ is within 11 % of the observed value. $\lambda 187.24$ is a known blend with Fe VII (Brown et al. 2008), and thus we can use the Fe VIII ratio to estimate a Fe VII contribution of 62.2 ± 4.2 erg $\text{cm}^{-2} \text{s}^{-1} \text{sr}^{-1}$, however Sect. 4 shows that this is inconsistent with the Fe VII atomic model. Note that the Fe VIII intensity predicted from the DEM shown in Table 4 of Paper I is significantly higher than that predicted from the branching ratio. This is because the DEM over-predicts the strength of the strong $\lambda 186.60$ line. $\lambda 196.65$ is a known blend (Brown et al. 2008; Young et al. 2009) with a Fe XII transition. Using the branching ratio to subtract the

Fe VIII component leaves an intensity of $50.2 \text{ erg cm}^{-2} \text{ s}^{-1} \text{ sr}^{-1}$ for Fe XII. Young et al. (2009) noted that the Fe XII $\lambda 196.64/\lambda 186.88$ ratio is relatively insensitive to density, and we find a value of 0.27 after the Fe VIII correction. In active regions where Fe XII is much stronger than Fe VIII, Young et al. (2009) found $\lambda 196.64/\lambda 186.88$ ratios of between 0.24 and 0.32, consistent with the value of 0.27 found here. This gives some confidence that the Fe VIII $\lambda 196.65/\lambda 197.36$ branching ratio is consistent with theory.

For the Group 2 and 3 ratios the theoretical values are evaluated as the averages of the ratios calculated over the density range $\log N_e = 8.0\text{--}10.0$ and temperature range $\log T = 5.65\text{--}5.95$, the former calculated at 0.1 dex intervals, and the latter at 0.05 dex intervals. The error on the theoretical value is set to be the 3σ variation of the ratio over the density and temperature ranges.

The Group 2 ratio $\lambda 192.01/\lambda 197.36$ involves lines emitted from the $3p^5 3d^2(^1S) ^2P$ term and Table 7 shows it is discrepant with theory. This is due to a blend of $\lambda 192.01$ with both a coronal line and a line from Fe VII (Sect. 4). Images formed in the line suggest the blending line is probably Fe XI and indeed Brown et al. (2008) list the $3s^2 3p^4 ^3P_1 - 3s^2 3p^3(^2D) 3d ^3S_1$ transition from this ion. This identification is questionable, though, given the inconsistent identifications from this upper level given by Brown et al. (2008): the decay to the ground 3P_2 level is listed at both 187.45 \AA and 188.30 \AA , and the decay to the ground 1D_2 level is listed at both 201.74 \AA and 202.70 \AA . Only the 187.45 and 201.74 \AA identifications are consistent with the 192.02 \AA line. The CHIANTI model for Fe XI has only a theoretical energy for the 3S_1 level, with the decay to 3P_1 level listed at 191.21 \AA . Using the Fe VIII $\lambda 192.01/\lambda 197.36$ theoretical ratio we estimate a contribution of $41.5 \pm 4.5 \text{ erg cm}^{-2} \text{ s}^{-1} \text{ sr}^{-1}$ of Fe VIII to the measured 192.01 \AA intensity. The remaining Group 2 ratios are discussed later in this section with regard the newly-identified $3p^6 3d ^2D_J - 3p^5 3d^2(^3F) ^4D_J^o$ transitions. Note that the strong lines from the $3p^5 3d^2(^3F) ^2F$ and $3p^6 4d ^2P$ terms show temperature and density sensitivity and so are not included in Table 7. $\lambda 185.21/\lambda 186.60$ was discussed earlier, while the ratio formed from lines from the $3p^6 4d ^2P$ term, $\lambda 195.97/\lambda 194.66$, has an observed ratio of 0.68 ± 0.01 which is very close to the high density limit of the theoretical ratio and implies a density $\log N_e \geq 8.64$, which is consistent with the Mg VII density value from Paper I.

The Group 3 ratios in Table 7 are formed from pairs of lines belonging to different multiplets. None of the ratios agrees with observations, although $\lambda 197.36/\lambda 194.66$ is only 10 % discrepant. The discrepancies for $\lambda 194.66/\lambda 185.21$ and $\lambda 197.36/\lambda 185.21$ are 60 and 77 % and suggest that the Fe VIII atomic model under-predicts the strength of the $\lambda 185.21$ line. The remaining Group 3 ratio is in better agreement with theory and is discussed below.

The theoretical Fe VIII model in CHIANTI predicts eight emission lines between 203

Table 7. Fe VIII insensitive ratios.

	Ratio	Theory	Observation ^a
Group 1	187.24 ^b / 186.60	0.046	0.097 ± 0.004
	196.65 ^c / 197.36	0.151	0.498 ± 0.014
	193.97 / 194.66	0.101	0.090 ± 0.004 ◀
Group 2	λ192.01 ^d / λ197.36	0.215 ± 0.023	0.398 ± 0.019
	λ255.13 / λ253.98	0.561 ± 0.064	0.395 ± 0.019 ◀
	λ255.37 / λ253.98	0.556 ± 0.111	0.678 ± 0.026
	λ255.71 / λ255.13	0.694 ± 0.099	0.500 ± 0.036 ◁
Group 3	λ197.36 / λ194.66	0.385 ± 0.015	0.422 ± 0.007 ◀
	λ194.66 / λ185.21	0.191 ± 0.033	0.305 ± 0.004 ◀
	λ197.36 / λ185.21	0.073 ± 0.013	0.129 ± 0.002 ◀
	λ206.75 / λ197.36	0.306 ± 0.070	0.261 ± 0.021

^aA ◁ symbol indicates a > 1σ discrepancy between theory and observation, ◀ indicates a > 2σ discrepancy.

^bBlended with Fe VII λ187.235.

^cBlended with Fe VII λ192.006 and an unknown hotter line.

^dBlended with Fe XII λ196.640.

Table 8. New Fe VIII level energies.

Level	Energy (cm ⁻¹)
$3p^5 3d^2(^3F) \ ^4D_{1/2}^o$	391 115 ± 6
$3p^5 3d^2(^3F) \ ^4D_{3/2}^o$	391 997 ± 6
$3p^5 3d^2(^3F) \ ^4D_{5/2}^o$	393 463 ± 12
$3p^5 3d^2(^3F) \ ^4D_{7/2}^o$	395 610 ± 12
$3p^5 3d^2(^3P) \ ^2D_{5/2}^o$	483 671 ± 10

and 208 Å, two of which are sufficiently strong to be easily observable in the present EIS spectrum. Firstly we note that the theoretical energies of Griffin et al. (2000) for the levels that give rise to the lines in the 185–200 Å range are all over-estimates of the experimental energies. If we assume the energies for the levels that give rise to the 203–208 Å lines are also over-estimated by a similar amount, then the lines should lie up to 4 Å longward of the theoretical wavelengths. The strongest lines predicted by CHIANTI are the $3p^63d\ ^2D_{5/2} - 3p^53d^2(^1G)\ ^2G_{7/2}^o$ transition at 203.08 Å and the $3p^63d\ ^2D_{3/2} - 3p^53d^2(^3P)\ ^2D_{5/2}^o$ transition at 205.01 Å, whose strengths should be 0.31 ± 0.07 and 0.26 ± 0.05 of the $\lambda 197.36$ Fe VIII line. A line at 206.78 Å is the best match, in terms of intensity, to the $^2G_{7/2}$ transition and we tentatively identify this transition. The image formed in the line is consistent with other Fe VIII images, and the Group 3 insensitive ratio, $\lambda 206.75/\lambda 197.36$, shown in Table 7 is consistent with theory. The new experimental energy for the $3p^53d^2(^1G)\ ^2G_{7/2}$ level is given in Table 8, and is derived assuming that a $+33\text{ km s}^{-1}$ wavelength shift applies to the Fe VIII lines as discussed earlier in this section. The error bar is derived using the measured centroid uncertainty, the EIS wavelength scale uncertainty of $\pm 0.002\text{ Å}$ (Brown et al. 2007), and the uncertainty of the Fe VIII velocity which is taken as the standard deviation of the six velocity measurements of the unblended Fe VIII lines (Table 6). Two lines at 208.68 and 208.84 Å could be the $3p^63d\ ^2D_{3/2} - 3p^53d^2(^3P)\ ^2D_{5/2}^o$ transition, however the former has a significant Cr VIII contribution (Paper I), while the latter is too strong to be completely due to Fe VIII. We thus do not make an identification for this transition in the spectrum.

Four emission lines between 253.9 and 255.8 Å that are normally weak become very prominent in the current spectrum. Their wavelengths and separations are close to those predicted by CHIANTI for four lines of the Fe VIII $3p^63d\ ^2D_J - 3p^53d^2(^3F)\ ^4D_J^o$ multiplet, for which only theoretical wavelengths are available, and images formed in the lines are very similar in morphology to the Fe VII and Fe VIII lines. We thus identify the observed lines with the Fe VIII transitions. The new experimental energy values for the 4D_J levels are given in Table 8 which have been derived in the same manner as the $3p^53d^2(^3P)\ ^2D_{5/2}$ discussed earlier. For the levels that decay to the excited $^2D_{5/2}$ level in the ground configuration, the $^2D_{5/2}$ energy of 1836 cm^{-1} of Ramonas & Ryabtsev (1980) has been used. An uncertainty of $\pm 10\text{ cm}^{-1}$ was assumed for this value.

Three ratios can be formed between the four lines that are relatively insensitive to density and temperature, and a comparison between observation and theory is shown in Table 7 (Group 2 lines). Only one of the three ratios agrees with theory within the error bars, but the disagreements are not large.

All four lines are predicted to show significant temperature sensitivity relative to the shorter wavelength lines between 185 and 200 Å. In particular we highlight the $\lambda 185.21/\lambda 255.34$

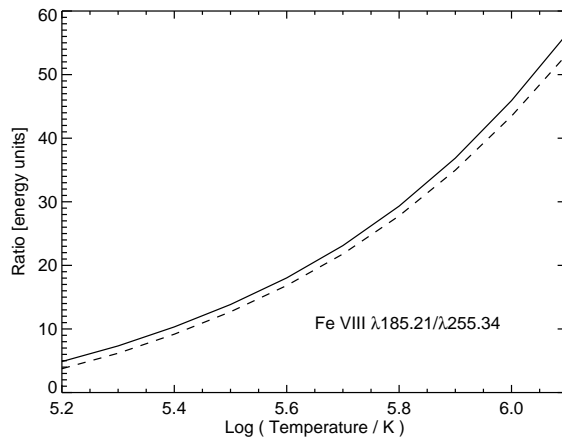


Fig. 7.— Theoretical variation of the $\lambda 185.21/\lambda 255.34$ ratio as a function of temperature. The ratio has been calculated for densities of 10^9 cm^{-3} (solid line) and 10^8 cm^{-3} (dashed line). There is little density sensitivity above 10^9 cm^{-3} .

ratio which shows very little density sensitivity, and the temperature variation is shown in Fig. 7. However, the observed ratio of 7.75 ± 0.23 gives a very low temperature of $\log T \approx 5.3$, well below the expected temperature of maximum ionization of Fe VIII (Sect. 3). This implies that the $\lambda 255.37$ line is observed to be around a factor 3–4 stronger than predicted by theory. It was noted earlier that insensitive ratios amongst the SW lines suggest that the CHIANTI model is under-estimating the strength of the $\lambda 185.21$ by 60–80 %. If this is the case, then the ratio curves plotted in Fig. 7 would be raised by this amount, making the derived $\lambda 185.21/\lambda 255.37$ temperature even lower.

This raises the question of whether the transitions between 254 and 256 Å actually are Fe VIII transitions. Firstly, we note that images formed in each line are consistent with other Fe VIII lines. The line separations are consistent with the theoretical energies of Griffin et al. (2000), and the observed wavelengths are within 1–2 % of the theoretical wavelengths. If the lines are not due to Fe VIII, then the transitions must be nearby in the spectrum, but a similar set of four lines with the correct intensities can not be found. The only other ion species that we believe can be responsible for the lines is Fe VII, but the observed lines are factors 5–10 stronger than the lines predicted from the Fe VII atomic model in this wavelength range.

Our conclusion is thus that the observed lines are the Fe VIII $3p^6 3d^2 D_J - 3p^5 3d^2 ({}^3F) {}^4D_J^o$ transitions but that the observed intensities do not match the Fe VIII atomic model. To fix the discrepancy would require the theoretical model to yield a greater level of excitation to the 4D levels. This can be achieved by cascading from higher levels or increased resonance excitation, both of which could be possible if the $3p^4 3d^3$ configuration is included in the

scattering calculation.

We summarise the results of the comparison between the Fe VIII atomic model and the EIS spectrum as follows.

- The $3p^6 3d^2 D_{5/2} - 3p^5 3d^2 ({}^1G) {}^2G_{7/2}^o$ has been identified at a rest wavelength of 206.753 Å leading to a new experimental value for the ${}^2G_{7/2}$ energy.
- Four transitions of the $3p^6 3d^2 D_J - 3p^5 3d^2 ({}^3F) {}^4D_J^o$ multiplet have been identified between 253.9 and 255.7 Å, leading to new experimental energies for the four 4D levels. The Fe VIII atomic model, however, underestimates the lines' strengths by a factor between 3 and 6.
- The two strong lines at 185.21 and 186.60 Å emitted from the $3p^5 3d^2 ({}^3F) {}^2F$ term are under-estimated by the atomic model by around 60–80 % compared to lines from the $3p^6 4d^2 P$ and $3p^5 3d^2 ({}^1S) {}^2P$ terms. In addition, the ratio of the two lines is discrepant with theory by around 10–20 %.
- The $\lambda 185.21/\lambda 255.34$ ratio is an excellent temperature diagnostic but yields temperatures significantly lower than expected due to the atomic data discrepancies highlighted above.
- The group of four nearby lines at 193.97, 194.66, 195.97 and 197.36 Å show good agreement. $\lambda 195.97/\lambda 194.66$ could be a useful density diagnostic in conditions where the density is $\leq 10^9 \text{ cm}^{-3}$.

The discrepancies highlighted above suggest that a new atomic calculation for Fe VIII is required. A new laboratory study of Fe VIII would also be valuable for classifying the large number of unidentified transitions between 200 and 260 Å.

6. Fe IX

The CHIANTI 5 atomic model was revised following the new line identifications of Young (2009) and is made available in CHIANTI 6 (Dere et al. 2009). The new model is described in more detail below and is compared with the Fe IX lines in the 2007 February 21 spectrum. In addition we highlight a number of observed lines that are likely to be due to Fe IX but for which definite transition identifications are not possible.

Four new Fe IX line identifications were performed by Young (2009) and the energy levels for the ion have been updated for CHIANTI 6 (Dere et al. 2009). The $3p^4 ({}^3P) 3d^2 {}^3G_J$ levels

were the first of the 109 levels of the $3p^4 3d^2$ configuration to be identified by any author, so they can be used to provide energy corrections to the entire set of $3p^4 3d^2$ levels. These lead to improved wavelength estimates for other transitions arising from the $3p^4 3d^2$ levels, a number of which are expected in the EIS SW band. Since only one level multiplet has been identified, the average difference between the experimental energies (from Young 2009) and theoretical energies (from Storey et al. 2002) has been calculated and subtracted from each of the other fine structure levels of the $3p^4 3d^2$ configuration. The energy subtracted is $43\,297\text{ cm}^{-1}$, and it shifts the predicted wavelengths by around 14 \AA compared to the values in CHIANTI 5.2 (Landi et al. 2006). This method of adjusting the level energies is very simplistic and the accuracy of the new wavelengths will not be high (perhaps a few \AA), but they should be more accurate than the previous estimates. The change in the Fe IX wavelengths following the energy shift is illustrated in Fig. 8. Of particular interest are a strong triplet arising from the $3p^4(^1D)3d^2\ ^3D_J$ levels between 177 and 180 \AA , and the group of weak lines between 188 and 199 \AA that lie in a wavelength region where the EIS sensitivity is high. Before considering these transitions, however, we discuss the previously-identified transitions.

The strong $\lambda 171.07$ resonance line is found at the extreme short wavelength end of the EIS SW band where the instrument effective area is very low. Despite this, the line is well-resolved and, when converted to calibrated intensity units, becomes almost a factor four stronger than every other line in the spectrum.

The four lines identified by Young (2009) are all found in the present spectrum. The strongest line, $\lambda 188.50$, is partially blended with weak lines in the short and long wavelength wings and is difficult to fit accurately as there is no nearby continuum level. The fit parameters shown in Paper I resulted from a simultaneous 15 Gaussian fit to lines between 187.71 and 189.13 \AA . A line in the short wavelength wing at 188.424 \AA is due to Fe VII and perhaps also a line of Mn IX (see the discussion in Paper 1), while another Fe VII line is found in the long wavelength wing at 188.603 \AA . $\lambda 189.94$ is partially blended with Fe X $\lambda 190.04$ but is easily resolved with a double-Gaussian fit. $\lambda 191.22$ and $\lambda 197.86$ are both unblended. The $\lambda 197.86/\lambda 171.07$ temperature diagnostic highlighted by Young (2009) yields a temperature of $\log T = 5.86 \pm 0.04$ which is in agreement with the T_{eff} value of 5.82.

The $3p^4(^3P)3d^2\ ^3G_{3,4}$ levels that give rise to the $\lambda 189.94$ and $\lambda 191.26$ lines also give rise to three weaker lines that are potentially observable in the present spectrum. 3G_4 decays to $3p^5 3d\ ^3F_3$ with expected wavelength of 188.686 \AA , and the branching ratio is 0.092 relative to $\lambda 189.94$. This line is observed in the spectrum with wavelength $188.685 \pm 0.007\text{ \AA}$, and the $\lambda 188.686/\lambda 189.941$ ratio is 0.134 ± 0.034 , within 2σ of theory. There is a S XI line expected at 188.675 \AA which blends with the Fe IX line, but using the calculated DEM gives a predicted

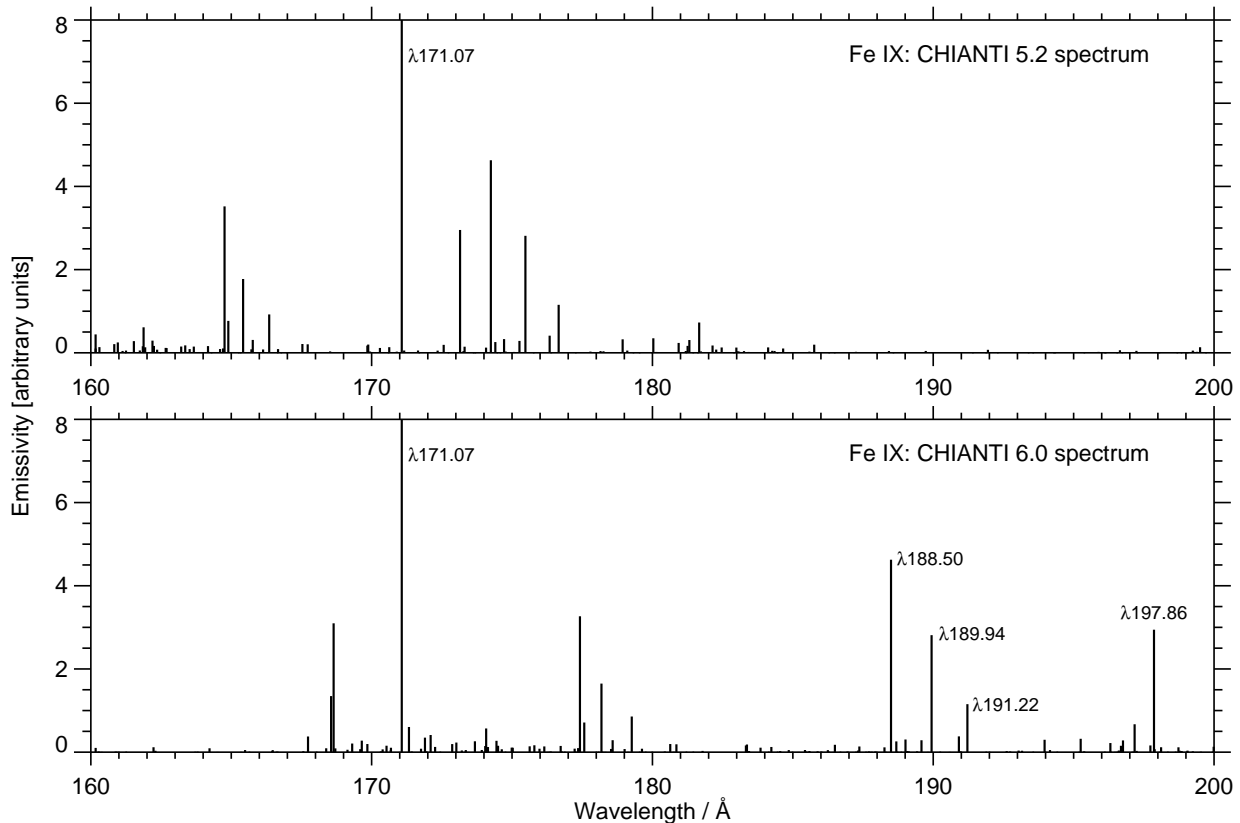


Fig. 8.— Theoretical Fe IX spectra calculated with CHIANTI 5.2 (top panel) and CHIANTI 6 (bottom panel). Each emission line is represented by a vertical line, the length of which corresponds to the line’s emissivity. The strong $\lambda 171.07$ line dominates, extending beyond the plots’ bounds to Y-values of 98. The four lines identified by Young (2009) are indicated in the bottom panel.

intensity of only $2.2 \text{ erg cm}^{-2} \text{ s}^{-1} \text{ sr}^{-1}$, therefore the Fe IX line dominates. An image formed in the 188.685 \AA line confirms that it is a blend of a cool line around the temperature of Fe IX and a hotter line.

The 3G_3 level gives rise to $\lambda 191.22$ and has six additional decays, two of which are potentially observable in the EIS spectrum. The strongest is the decay to $3p^5 3d {}^3F_3$ at 189.582 \AA , with a branching ratio of 0.248. It is a good wavelength match to an observed line at 189.596 \AA , but the observed ratio is significantly lower than theory at 0.076 ± 0.016 . The image formed in the line, however, is consistent with a formation temperature close to Fe IX. The next strongest line from 3G_3 is the decay to $3p^5 3d {}^1D_2$ at 199.986 \AA with a branching ratio of 0.112. This line is blended with Fe XIII $\lambda 200.02$ and contributes around 25 % to the observed feature (Paper I). The image formed in this line is dominated by the

Fe XIII component, however a weak cool component can be identified, particularly if the image is formed in the short wavelength wing of the line.

The $3p^5 3d \ ^3F_J - 3p^4(^1D)3d^2 \ ^3D_{J-1}$ ($J = 4, 3, 2$) triplet of lines is predicted at 177.419, 178.185 and 179.263 Å, and are the strongest of the predicted lines between $\lambda 171.07$ and $\lambda 188.50$ (see bottom panel of Fig. 8). Although the lines are comparable in strength to the longer wavelength triplet, the EIS effective area is much lower around 177–180 Å making the lines more difficult to identify. A good candidate for the stronger line is the observed line at 176.968 Å. It contains a Fe VII component, but Sect. 4 demonstrated that this transition makes a contribution of 30 %. The remaining intensity of $313 \pm 51 \text{ erg cm}^{-2} \text{ s}^{-1} \text{ sr}^{-1}$ is consistent with the theoretical $\lambda 177.419$ line: the $\lambda 177.419/\lambda 188.50$ theoretical ratio is ≈ 0.7 , giving a predicted intensity of $263 \text{ erg cm}^{-2} \text{ s}^{-1} \text{ sr}^{-1}$ using the measured $\lambda 188.50$ intensity.

With this identification the $^3F_3 - ^3D_2$ transition can be tentatively identified with the observed 177.603 Å line based on wavelength separation and expected intensity. The theoretical $\lambda 178.185/\lambda 177.419$ ratio is 0.51 for a density of 10^9 cm^{-3} which, using the estimated intensity of the measured 176.968 Å line above, yields a predicted intensity of $160 \text{ erg cm}^{-2} \text{ s}^{-1} \text{ sr}^{-1}$ in excellent agreement with the measured line intensity (Paper 1). Brown et al. (2008) identified a line seen in quiet Sun and active region spectra at this wavelength with S X $\lambda 177.545$ and Ni XIV $\lambda 177.560$, however, using the DEM distribution we can demonstrate that these lines each contribute less than $1 \text{ erg cm}^{-2} \text{ s}^{-1} \text{ sr}^{-1}$ to the observed line at 177.603 Å. Based on wavelength separation and predicted intensity, there are two candidates for the theoretical $\lambda 179.263$ line ($^3F_2 - ^3D_1$ transition): the measured lines at 178.708 and 178.994 Å. The line is expected to be a factor 0.27 weaker than $\lambda 177.419$ which is consistent with both lines' measured intensities. We note that the Fe IX transition $3p^5 3d \ ^3D_3 - 3p^4(^3P)3d^2 \ ^3F_4$ has a predicted wavelength of 177.572 Å and a predicted intensity around 80 % of $\lambda 179.263$ thus it could account for one of the two observed lines.

In summary, we identify the observed 176.968 and 177.603 Å lines with the 4–3 and 3–2 components of the $3p^5 3d \ ^3F_J - 3p^4(^1D)3d^2 \ ^3D_{J-1}$ triplet, but do not make an identification for the 2–1 component. New experimental energies for the $3p^4(^1D)3d^2 \ ^3D_{2,3}$ levels are given in Table 9. The values have been derived by adjusting the measured wavelengths by the average velocity shift of the $\lambda 188.50$, $\lambda 189.94$, $\lambda 191.22$ and $\lambda 197.86$ lines ($+16 \text{ km s}^{-1}$), and the uncertainties are a combination of the measured wavelength uncertainties, the uncertainties of the four reference wavelengths, and the uncertainties of the lower level energies (see Young 2009, for more details). An updated theoretical energy for the 3D_1 level is also given in Table 9 and is derived from the new $^3D_{2,3}$ energies by determining the average difference in theoretical and experimental energies for these levels and subtracting this from

the theoretical 3D_1 energy.

No other Fe IX lines can be definitively identified from the EIS spectrum. However, Table 10 gives a list of measured lines that we believe are due to Fe IX or have a component due to Fe IX. The lines have been identified through comparisons of their image intensity distributions as described in Paper I, and also by comparing the Paper I spectrum with that of Young (2009) which shows stronger Fe IX emission relative to Fe VII and Fe VIII and so is valuable for discriminating between these three ions for weak lines.

Table 11 gives a list of the six strongest unidentified lines in the range 170–212 Å which are thus the best candidates for the suggested Fe IX lines in Table 10. The intensities are presented relative to $\lambda 197.86$, computed for a temperature of $\log T = 5.8$ and density $\log N_e = 9.0$. A short hand notation is used so that ${}^3P_2-({}^3P){}^3D_3$, for example, corresponds to the transition $3p^53d\ {}^3P_2 - 3p^4({}^3P)3d^2\ {}^3D_3$. The strongest of the six theoretical transitions is $\lambda 197.174$, and we note that a further decay from this line’s upper level is to the $3p^53d\ {}^3F_4$ level with a branching ratio of 0.267. Identifying $\lambda 197.174$ with the strongest of the observed lines at 194.816 Å implies the decay to 3F_4 occurs at 199.536 Å which is close to the observed 199.613 Å line. However, the difference in wavelength (corresponding to 117 km s $^{-1}$) is too large given the accuracy of the measured EIS wavelengths and the $3p^53d$ energy levels (Edlén & Smitt 1978), and so we do not identify the observed 194.816 Å line with the line of theoretical wavelength 197.174 Å.

Identifying the $\lambda 197.174$ theoretical line with the observed line at 192.642 Å would imply the decay to 3F_4 would occur at 197.255 Å, however no observed line is found at this wavelength. Finally if $\lambda 197.174$ was identified with the observed line at 187.971 Å, then the 3F_4 decay would be found at 192.361 Å. This latter line would blend with Fe XII $\lambda 192.39$ and we note that a line is found in the short wavelength wing of this line at 192.313 Å, however this is 75 km s $^{-1}$ away from the expected position of the Fe IX line and so the identification can not be made.

Since no positive identification can be made for the strongest of the six lines in Table 11, then we do not attempt to find identifications for the remaining lines. A new laboratory study that can clearly separate Fe IX lines from the numerous blending species found in the solar spectrum would be extremely valuable for further classifying the many Fe IX lines in the 170–200 Å wavelength range.

Table 9. New Fe IX level energies.

Level	Index ^a	Energy (cm ⁻¹)
$3p^4(^1D)3d^2\ ^3D_3$	110	990913 ± 24
$3p^4(^1D)3d^2\ ^3D_2$	111	992393 ± 30
$3p^4(^1D)3d^2\ ^3D_1$	112	993321 ^b

^aIndex of the level in the CHIANTI 6 Fe IX atomic model.

^bEnergy derived from theoretical level splittings.

Table 10. Possible Fe IX emission lines.

Wavelength (Å)	Intensity (erg cm ⁻² s ⁻¹ sr ⁻¹)	Class ^a
186.004	18.5	C–E
187.971	89.8	E
192.642	76.7	E–F
194.816	109.0	C–E
195.753	20.2	E,G–H
196.820	35.0	E–G
199.613	34.4	E–F

^aSee Table 1 of Paper I.

7. Effects on response functions of EUV imaging instruments

Solar EUV imaging instruments such as SOHO/EIT, TRACE and SECCHI/EUVI employ multilayer optical coatings to pick out narrow wavelength regions centered on specific EUV emission lines. For example, each of these instruments has a channel centered on the $\lambda 195.12$ line of Fe XII. Although images formed in this channel are dominated by Fe XII and thus principally reveal plasma at temperatures of 1.5 MK, many other emission lines within $\approx \pm 10 \text{ \AA}$ contribute to the channel and can modify the response of the channel to temperature. For example, observations of flares with TRACE (Gallagher et al. 2002) have shown that the 195 channel becomes dominated by Fe XXIV $\lambda 192.03$ (formed at 20 MK) in the flare region, while Del Zanna et al. (2003) showed that lines of Fe VIII, Fe X and Fe XI make a significant contribution to polar plume emission.

To determine the response of an EUV imaging channel to plasma temperature it is necessary to compute synthetic spectra for a set of isothermal plasmas using an atomic code. By convolving the synthetic spectra with the instrument response function, one can predict the instrument signal as a function of temperature. Since different wavelength channels will have different responses to temperature, then ratios formed from the channels (referred to as filter ratios) can be used to determine the plasma temperature (Moses et al. 1997). This method depends critically on the completeness of the atomic models. For example, for the TRACE satellite the CHIANTI atomic database was used to derive the instrument response function but, prior to the version 3 release (Dere et al. 2001), CHIANTI contained no atomic data for Fe VIII which led to the errors in the response function for the 195 channel highlighted by Del Zanna & Mason (2003).

For this work a new atomic model for Fe VII has been prepared that predicts many new lines in the EUV that were not previously included in CHIANTI. In addition, the Fe IX model has been revised significantly since the version 5.2 CHIANTI release (Landi et al. 2006) with new lines identified and many lines with theoretical wavelengths shifted to new wavelengths. The present section investigates the effects on response functions for the TRACE instrument.

The TRACE response functions currently in Solarsoft were derived using CHIANTI 5. To investigate the effects of the new Fe VII and Fe IX models we use CHIANTI 5 with the Fe VII and Fe IX data replaced with the new data. We use software developed by Brooks & Warren (2006) that derives the TRACE filter responses as a function of temperature using the CHIANTI spectra.

The left and middle panels of Fig. 9 show the revised response functions for the TRACE 173 and 195 channels. The 173 channel has a greater sensitivity to Fe X $\lambda 174.53$ than Fe IX

$\lambda 171.07$ and so the curve peaks at the T_{\max} of Fe X. The Fe IX lines between 170 and 180 Å shown in the lower panel of Fig. 8 make a small increase to the response function, particularly the $3p^5 3d \ ^3F_J - 3p^4(^1D)3d^2 \ ^3D_{J-1}$ ($J = 4, 3, 2$) transitions discussed in Sect. 6. Many Fe VII lines between 170 and 180 Å also increase the response function, with the $3p^6 3d^2 \ ^3F_J - 3p^5 3d^3(^4F) \ ^3F_J$ ($J = 2, 3, 4$) transitions making the largest contribution.

The 195 channel response function shows a much greater change. In particular a dip in the function that occurred at $\log T = 5.8$ disappears due to the many Fe IX lines now found between 188 and 200 Å that were previously absent. The Fe VII lines between 195 and 197 Å also make a significant increase to the response function around $\log T = 5.4$ – 5.7 .

Forming a ratio of the 173 and 195 channel response functions yields the function shown in the right panel of Fig. 9. Although significant structure is seen, the most important feature is the fall between $\log T = 5.8$ to 6.3 which is the temperature range where Fe IX, Fe X and Fe XII are formed. Since in most coronal conditions these ions dominate the channels' emission, then the slope means that the channel ratio 173/195 can be used to diagnose temperatures in the range $\log T = 5.8$ – 6.3 . This feature was first exploited for the SOHO/EIT instrument (Moses et al. 1997) which has very similar channels to TRACE, and has been used in a number TRACE analyses, particularly studies of coronal loops (Lenz et al. 1999; Aschwanden et al. 2000). Comparing the curves derived with CHIANTI 5.2, with and without the new Fe VII and Fe IX data, shows a significant change to the response function ratio at $\log T = 5.9$: the new ratio curve is a factor 2.3 lower than previously. For $\log T \geq 6.0$, however, the change is ≤ 20 %.

8. Summary

Eleven new line identifications have been performed for Fe VII, leading to the assignment of eight new experimental energies for the $3p^5 3d^3$ configuration, and the revision of two level assignments. Four new line ratio diagnostics for temperature and density have been highlighted, although discrepancies with values obtained through other methods were found. Good agreement with theory is found for around half of the Fe VII lines, but there are many discrepancies of up to a factor two. The problems are most likely due to the atomic data for this complex ion, but a new laboratory study of Fe VII would be valuable, particularly for confirming line identifications.

Five new line identifications have been performed for Fe VIII, leading to five new experimental energies in the $3p^5 3d^2$ configuration. Comparing observed line intensities with theory has revealed a number of problems for the Fe VIII ion. The strong transitions between 185

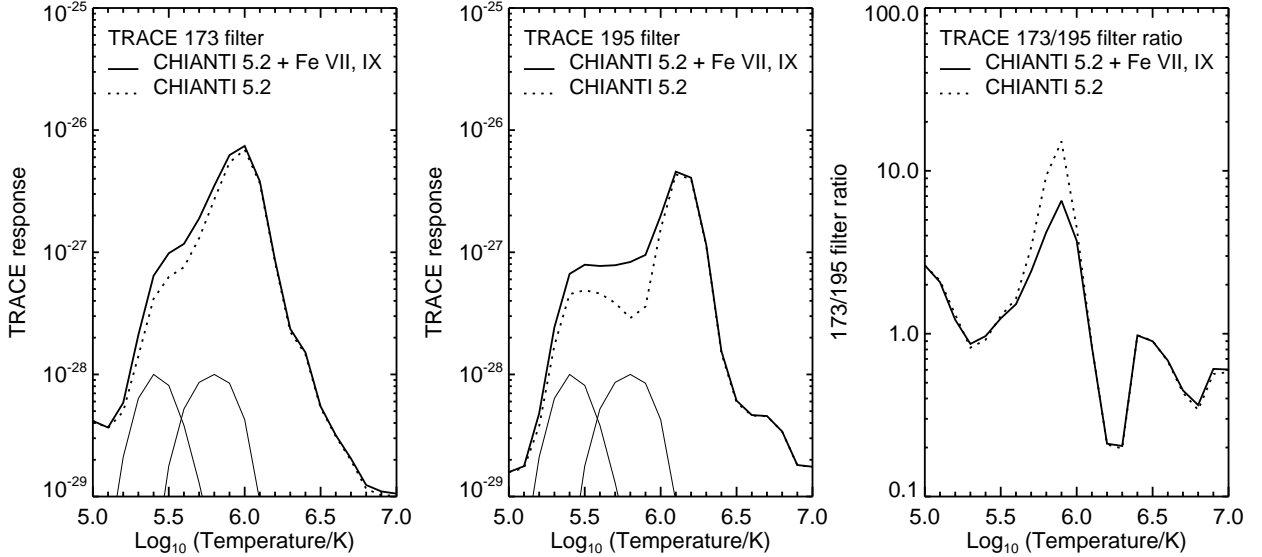


Fig. 9.— The left and middle panels compare the response functions computed with CHIANTI 5.2 (dotted line) and CHIANTI 5.2 supplemented with the new Fe VII and Fe IX atomic data (solid line) for the 173 and 195 channels, respectively. The functions are increased by the new data in the $\log T = 5.5\text{--}6.0$ region, particularly for 195. At the bottom of both plots are shown the ionization fraction curves for Fe VII and Fe IX (from Mazzotta et al. 1998) to show their ranges of formation. The right panel plots the 173/195 filter ratio (which is used to derive plasma temperatures). The new curve is lower by up to a factor 3 over the region $\log T = 5.5\text{--}6.0$.

and 187 \AA arising from the $3p^5 3d^2(^3F) ^2F$ term are not consistent with the lines between 192 and 198 \AA emitted from the $3p^6 4d ^2P$ and $3p^5 3d^2(^1S) ^2P$ terms, being under-predicted by the atomic model by 60–80 %. In addition, the newly identified multiplet from the $3p^5 3d^2(^3F) ^4D$ term around $253\text{--}256 \text{ \AA}$ is observed to be stronger than predicted by theory by factors of between 3 to 6 compared to the lines in the EIS SW wavelength band. A new atomic study would be valuable for investigating these problems, while a new laboratory study of Fe VIII between 170 and 260 \AA is required to identify the many identified transitions in this range.

Young (2009) identified the four strongest Fe IX lines in the EIS spectra and additional identifications have been performed here. In addition, a number of emission lines have been classed as Fe IX lines based on image morphology but specific atomic transitions could not be assigned. A laboratory study of Fe IX lines around $160\text{--}200 \text{ \AA}$ is required to make further progress.

Solar EUV imaging instruments such as SOHO/EIT, TRACE, STEREO/EUVI and the upcoming SDO/AIA require accurate atomic models for modeling the dependence of

the instruments' filters to plasma temperature. Using the new atomic data and line identifications of Fe VII–IX we have modeled the TRACE 173 and 195 filter response functions, demonstrating a significant change to the 195 filter response at temperatures $\log T = 5.4$ – 6.0 . This leads to a modification of the TRACE 173/195 filter ratio that can affect coronal temperature determinations.

The work of EL is supported by the NNG06EA14I, NNH06CD24C and other NASA grants. Hinode is a Japanese mission developed and launched by ISAS/JAXA, with NAOJ as domestic partner and NASA and STFC (UK) as international partners. It is operated by these agencies in co-operation with ESA and NSC (Norway).

REFERENCES

- Arnaud, M., & Rothenflug, R. 1985, *A&ASS*, 60, 425
- Arnaud, M., & Raymond, J.C. 1992, *ApJ*, 398, 394
- Aschwanden, M. J., Nightingale, R. W., & Alexander, D. 2000, *ApJ*, 541, 1059
- Bromage, G. E., Cowan, R. D., & Fawcett, B. C. 1977, *Phys. Scripta*, 15, 177
- Brooks, D. H. & Warren, H. P. 2006, *ApJS*, 164, 202
- Brown, C. M., Hara, H., Kamio, S., et al. 2007, *PASJ*, 59, S865
- Brown, C. M., Feldman, U., Seely, J. F., Korendyke, C. M., & Hara, H. 2008, *ApJS*, 176, 511
- Bryans, P., Badnell, N.R., Gorczyca, T.W., Laming, J.M., Witthumsiri, W., & Savin, D.W. 2006, *ApJS*, 167, 343
- Bryans, P., Landi, E., & Savin, D. W. 2009, *ApJ*, 691, 1540
- Culhane, J. L., Harra, L. K., James, A. M., et al. 2007, *Solar Physics*, 243, 19
- Czyzak, S. J., & Krueger, T.K. 1966, *ApJ*, 144, 381
- Delaboudinière, J.-P., Artzner, G. E., Brunaud, J., et al. 1995, *Sol. Phys.*, 162, 291
- Del Zanna, G. & Mason, H. E. 2003, *A&A*, 406, 1089
- Del Zanna, G., Bromage, B. J. I., & Mason, H. E. 2003, *A&A*, 398, 743

- Del Zanna, G., Berrington, K. A., & Mason, H. E. 2004, *A&A*, 422, 731
- Dere, K. P., Landi, E., Mason, H. E., Monsignori-Fossi, B. C., & Young, P. R. 1997, *A&AS*, 125, 149
- Dere K. P., Landi E., Young P. R., & Del Zanna G. 2001, *ApJS*, 134, 331
- Dere K. P., Landi E., Young P. R., et al. 2009, *A&A*, 498, 915
- Edlén, B., & Smitt, R. 1978, *Sol. Phys.*, 57, 329
- Ekberg, J. O. 1981, *Phys. Scripta*, 23, 7
- Ekberg, J. O., & Feldman, U. 2003, *ApJS*, 148, 567
- Gabriel, A. H., Fawcett, B. C., & Jordan, C. 1966, *Proc. Phys. Soc.*, 87, 825
- Gallagher, P. T., Dennis, B. R., Krucker, S., Schwartz, R., & Tolbert, A. K. 2002, *Sol. Phys.*, 210, 341
- Griffin, D. C., Badnell, N. R., Pindzola, M. S., & Shaw, J. A. 1998, *J. Phys. B*, 31, 3713
- Griffin, D. C., Pindzola, M. S., & Badnell, N. R. 2000, *A&AS*, 142, 317
- Gu, M. F. 2003, *ApJ*, 582, 1241
- Handy, B. N., Acton, L. W., Kankelborg, C. C. et al. 1999, *Sol. Phys.*, 187, 229
- Harrison, R. A., Sawyer, E. C., Carter, M. K., et al. 1995, *Sol. Phys.*, 162, 233
- Howard, R. A., Moses, J. D., Vourlidas, A., et al. 2008, *Space Sci. Rev.*, 136, 67
- Keenan, F. P., Jess, D. B., Aggarwal, K. M., et al. 2008, *MNRAS*, 389, 939
- Landi, E., Del Zanna, G., Young, P.R. et al. 2006, *ApJS*, 162, 261
- Landi, E., & Young, P. R. 2009, *ApJ*, submitted
- Lenz, D., DeLuca, E. E., Golub, L., Rosner, R., & Bookbinder, J. A. 1999, *ApJ*, 517, L155
- Mazzotta, P., Mazzitelli, G., Colafrancesco, S., & Vittorio, N. 1998, *A&AS*, 133, 403
- Moses, D., Clette, F., Delaboudinière, J.-P., et al. 1997, *Sol. Phys.*, 175, 571
- Phillips, K. J. H., Feldman, U., & Landi, E. 2008, *Ultraviolet and X-ray Spectroscopy of the Solar Atmosphere*, CUP, 2008

- Ralchenko, Yu., Kramida, A. E., Reader, J., et al. 2008, NIST Atomic Spectra Database (version 3.1.5), [Online]. Available: <http://physics.nist.gov/asd3> [2009, July 17]. National Institute of Standards and Technology, Gaithersburg, MD
- Ramonas, A. A., & Ryabtsev, A. N. 1980, *Opt. Spect.*, 48, 348
- Raymond, J. C., & Doyle, J. G. 1981, *ApJ*, 247, 686
- Shull, J.M., & Van Steenberg, M. 1982, *ApJS*, 48, 95 and *ApJS*, 49, 351
- Storey, P. J., Zeippen, C. J., & Le Dourneuf, M. 2002, *A&A*, 394, 753
- Witthoeft, M. C., & Badnell, N. R. 2008, *A&A*, 481, 543
- Young, P. R., Del Zanna, G., Mason, H. E., et al. 2007a, *PASJ*, 59, S857
- Young, P. R., Del Zanna, G., Mason, H. E., et al. 2007b, *PASJ*, 59, S727
- Young, P. R. 2009, *ApJ*, 691, L77
- Young, P. R., Watanabe, T., Hara, H., & Mariska, J. T. 2009, *A&A*, 495, 587
- Zeng, J., Liang, G. Y., Zhao, G., & Shi, J. R. 2005, *MNRAS*, 357, 440

Table 11. Predicted Fe IX intensities relative to $\lambda 197.86$.

Transition	Wavelength (\AA)	Ratio ^a	Predicted intensity ($\text{erg cm}^{-2} \text{s}^{-1} \text{sr}^{-1}$)
$^3P_2-(^3P)^3D_3$	197.174	0.260	49
$^3D_3-(^1S)^3F_4$	190.913	0.140	26
$^3D_2-(^1S)^3F_3$	195.250	0.121	23
$^1F_3-(^1D)^1G_4$	189.012	0.119	22
$^3D_3-(^3P)^1G_4$	193.965	0.112	21
$^1D_2-(^1D)^1F_3$	196.758	0.110	21

^aRelative to $\lambda 197.86$.